GEOLOGY OF THE SHACKLETON RANGE: I. THE SHACKLETON RANGE METAMORPHIC COMPLEX

By PETER D. CLARKSON

ABSTRACT. The Shackleton Range Metamorphic Complex forms the Precambrian basement to the Shackleton Range. It is broadly divided into two parts: older gneisses with migmatites and granite stocks, and a younger metasedimentary sequence of schists, amphibolites and metalimestones. Two structural trends, related to the two periods of metamorphism, are recognized but the relationship between the rocks of each period is not known. The petrology of the major rock types is described.

Fifty-nine chemicals analyses of migmatite neosomes and related rocks are given to demonstrate the evolution of the migmatites. A period of anatexis with increasing temperature, accompanied by continual draining of a "magma chamber", produced an initial acid magma which became more basic with time. The final event in the anatectic sequence was the intrusion of a granodiorite dyke.

THE Shackleton Range (lat. 80°07′–80°50′S, long. 31°–19°W) lies east of the Filchner Ice Shelf at the head of the Weddell Sea (Clarkson, 1972). The Shackleton Range Metamorphic Complex forms the Precambrian basement and is exposed throughout most of the range (Fig. 1). It comprises older gneisses which have been migmatized and intruded by granite stocks and a younger metasedimentary sequence of schists, amphibolites and metalimestones. The basement complex is overlain in the south by the late Precambrian Turnpike Bluff Group of slates and quartzites (Clarkson, 1982*a*) and in the north-west by the Cambro-Ordovician Blaiklock Glacier Group of arenaceous rocks (Clarkson and Wyeth, 1982). Dolerite dykes were intruded during the Ordovician, Carboniferous (Rex, 1971) and Mesozoic (Clarkson, 1982*b*).

The Shackleton Range Metamorphic Complex has been broadly divided into two parts: the older gneisses, which have been extensively migmatized and intruded by granitic stocks, crop out mainly in the Read Mountains, Otter Highlands and parts of the Haskard Highlands; the younger schists, amphibolites and metalimestones represent a metamorphosed sedimentary sequence cropping out in the northern part of the range and in the central part of the Haskard Highlands. Within each of these broad areas are contrasting inliers and outliers but their contact relationships are not known, although faulting or thrusting seem likely.

The older part of the Shackleton Range Metamorphic Complex is considered to be Middle Precambrian; a granodiorite dyke, the final expression of the migmatization, intruding the granite at Hatch Plain, has been dated at 1 446±60 Ma (Rex, 1971), thereby providing a minimum age for the migmatization. The age of the metasedimentary sequence is not known.

The nearest similar rocks to the Shackleton Range Metamorphic Complex are found in Heimefrontfjella (Worsfold, 1967; Thomson, 1968; Juckes, 1972) and in areas farther east (Roots, 1953, 1969) but detailed comparison between these rocks and those of the Shackleton Range has not been made. However, it seems likely that the older part of the Shackleton Range Metamorphic Complex represents part of the Antarctic shield.

STRUCTURE

The structure of the gneisses and migmatites forming the older part of the basement complex is not clearly defined. In the western part of the range a north-west plunging fold axis is indicated (Fig. 2a) and this agrees fairly closely with the few observed fold axes. In the Read Mountains the distribution of poles to foliation planes (Fig. 2b) suggests either a possible north–south fold trend or an east–west fold trend. However, it is also possible that these rocks originally had a north-west to south-east trend, which has been modified subsequently

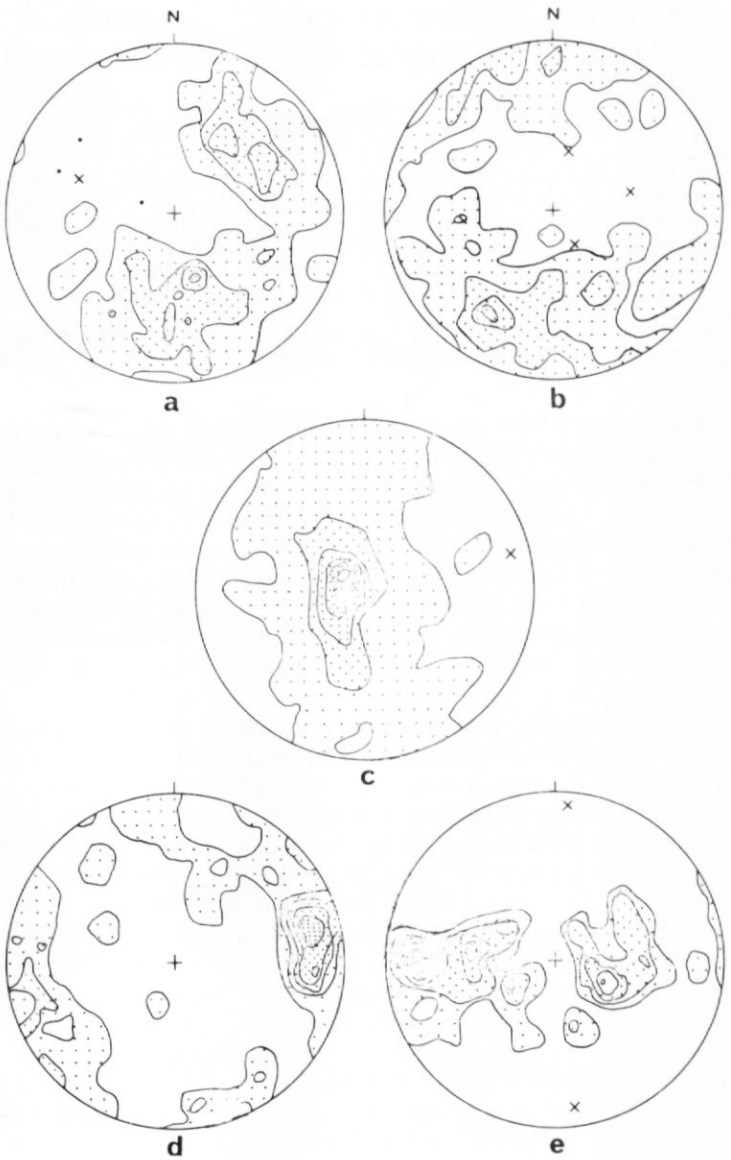

Fig. 2. Structural stereograms of rocks in the Shackleton Range Metamorphic Complex. The contours are at 0, 2½, 5, 7½, 10 and 20% per 1% unit area.

● Plunge of observed fold axis.

× Plunge of calculated fold axis.

a. Poles to foliation planes in gneisses and migmatites from northern and southern Haskard Highlands and central Otter Highlands.

b. Poles to foliation planes in gneisses and migmatites in the Read Mountains.

c. Poles to foliation planes in schists, amphibolites and metalimestones from the Lagrange Nunataks, the Herbert Mountains and Pioneers Escarpment.

d. Plunges of fold axes in schists, amphibolites and metalimestones from the Lagrange Nunataks, the Herbert Mountains and Pioneers Escarpment.

e. Poles to foliation planes in schists, amphibolites and metalimestones from central Haskard Highlands.

during migmatization, culminating in the intrusion of the granite stocks and consequent steepening of the fold limbs.

Folding of the younger metasedimentary sequence of the basement complex was about predominantly east–west fold axes. This is illustrated by the stereogram of poles to foliation planes (Fig. 2c) where the calculated fold axial plunge is coincident with the maximum concentration of observed fold axial plunges (Fig. 2d). Some evidence of north–south folding is shown by the observed fold axes (Fig. 2d) and also by the plot of poles to foliation planes in the metasedimentary rocks of central Haskard Highlands (Fig. 2e). This trend is regarded as the local expression of the Cambro-Ordovician Ross orogeny.

The predominant east–west fold trend of the Shackleton Range Metamorphic Complex continued through the Precambrian, where it is most obvious in the Turnpike Bluff Group (Clarkson, 1981*a*), and is evident at the present time in the shape of the range shown by the trend of the major boundary fault zones now occupied by Slessor and Recovery Glaciers. This trend may still be active if the report of an earthquake at approximately lat. 80°S, long. 20°W (Kaminuma and Ishida, 1971) is related to the northern boundary fault zone beneath Slessor Glacier.

Schists

Several varieties of schist have been found in the Shackleton Range and they are described here under seven broad headings according to their principal ferromagnesian minerals or metamorphic index minerals. Most of these schists have a wide distribution except for certain garnet-mica-schists, which are very distinctive in the hand specimen, and the pyroxene-schists, which appear to be confined to the Dutoit Nunataks and the area around Mount Provender (Stephenson, 1966).

Pyroxene-schists

These are among the highest grade schists in the range and are associated, at the Dutoit Nunataks, with high-grade gneisses, migmatites and granite. In thin section these rocks have a granular texture with slight elongation and comprise crystals of pyroxene and feldspar with accessory quartz, kyanite, brown biotite, pink sphene and rare unidentified ore minerals. The pyroxene is colourless or slightly pale green with a maximum extinction angle ($\gamma : c = 49°$) indicating augite. It is normally fresh although some crystals are partly altered and replaced by cryptocrystalline sericite or calcite. Plagioclase is the principal feldspar which is usually fresh and polysynthetically twinned. In the thin section of specimen Z.682.1 (Fig. 3a) the plagioclase is labradorite (An_{55}), whereas in specimen Z.688.2 there is much microcline, some very heavily sericitized, and the plagioclase is andesine (An_{28}). An additional contrast between these two rocks is the presence of biotite and kyanite in specimen Z.682.1 against sphene and a trace of biotite in specimen Z.688.2. These mineralogical differences may depend on the partial pressure of water, greater in specimen Z.682.1, although their bulk chemical compositions could be similar. Despite their pyroxene content, these rocks must belong to the hornblende-granulite facies as sphene is invariably absent from the pyroxene-granulite facies (Turner and Verhoogen, 1960).

Hornblende-schists

These schists are possibly the commonest in the Shackleton Range. They consist essentially of a quartzo-feldspathic mosaic with crystals of hornblende and often biotite marking the schistosity (Fig. 3b). Accessory minerals include garnet, epidote, sphene, zircon, calcite, muscovite and ore minerals.

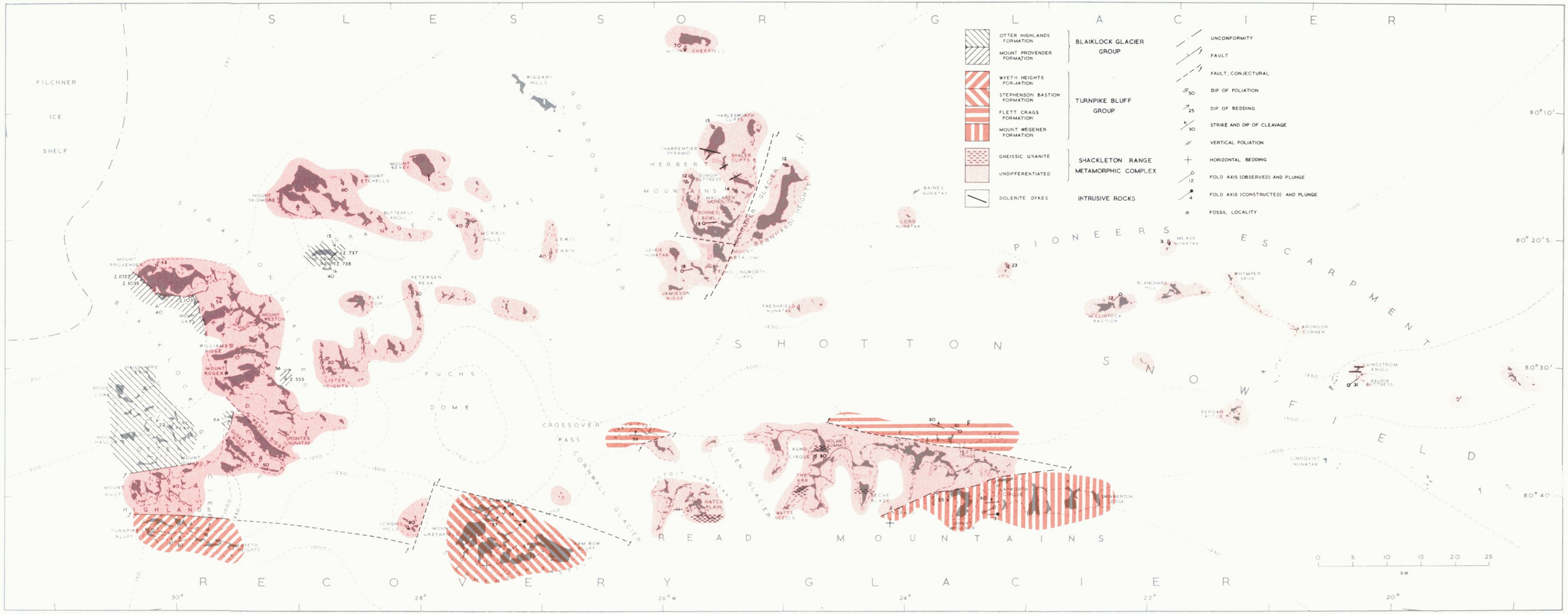

Fig. 1. Generalized geological sketch map of the Shackleton Range showing the outcrop of the major rock groups.

face page 258

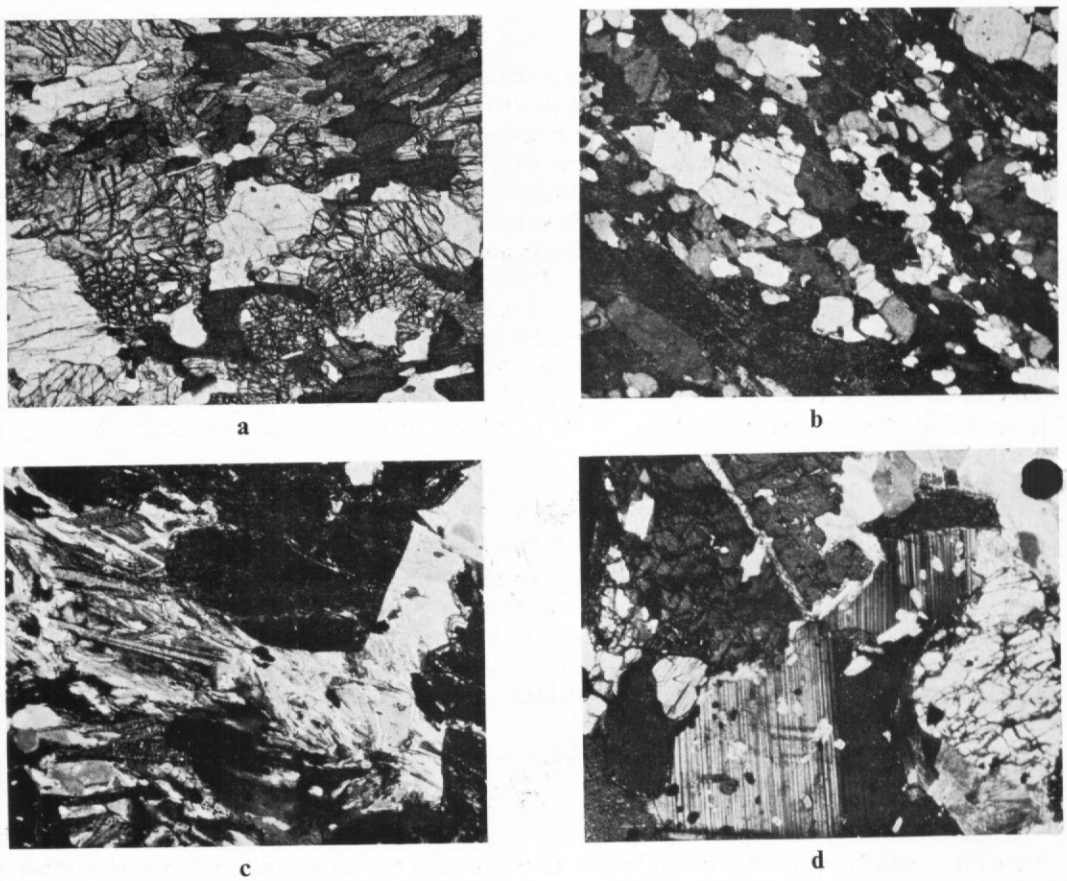

Fig. 3. a. Augite, biotite and labradorite in a pyroxene-schist (Z.682.1; ordinary light; ×27).
b. Intergrown biotite and hornblende marking the schistosity in the quartzo-feldspathic matrix of a hornblende-schist (Z. 724.1; X-nicols; ×27).
c. Muscovite and biotite wrapped around a garnet with quartz inclusions in a garnet-mica-schist (Z.585.8; X-nicols; ×30).
d. Staurolite, kyanite and biotite against garnet in a staurolite-kyanite-schist (Z.657.1; X-nicols; ×30).

Quartz is the principal mineral in most thin sections, occurring as equant to elongate crystals with sutured margins. Most crystals are strained to some degree but the quartz mosaic in lenses invariably shows the greatest strain. Inclusions are rare but lenses often contain long, thin orientated plates of mica.

The feldspars show considerable variation in composition. Plagioclase is commonest, frequently untwinned and difficult to determine but albite twins, where present, and optic signs indicate a variation from albite (An_8) to andesine (An_{34}). These feldspars are usually fresh, whereas those thin sections with potash feldspar, typically microcline, also show many untwinned crystals which are heavily sericitized. Many feldspars are microperthitic but the host is unknown; these often show the greatest degree of sericitization. Myrmekite occurs in some thin sections.

Hornblende usually has a pleochroism scheme α = pale brown, β = green, γ = dark blue-green. It occurs as interstitial xenomorphic crystals in the quartzo-feldspathic matrix and is often intergrown with biotite, sometimes in sandwich form. Laths are rarely longer than

1 mm and usually comprise up to 10% of the thin section. There seems to be little gradation between the hornblende-schists and the amphibolites with 50% or more hornblende.

Mica in these rocks is usually biotite, either a dark green-brown variety or common brown biotite. Alteration to pale green penninite is common along crystal margins and cleavage traces. It tends to form in bands which mark the schistosity. Muscovite occurs to a minor extent in some thin sections and is always unaltered.

Garnet is uncommon but it occurs as xenomorphic porphyroblasts, often shattered, partly altered to chlorite and embayed by epidote with inclusions of quartz and zircon. There is no evidence of rotation. Epidote commonly occurs as minute crystals (0.1 mm or less) in the matrix. Sphene, zircon, calcite and ilmenite are found in accessory or trace amounts in most thin sections.

Mica-schists

These schists also have a wide distribution. Most thin sections have a quartz or quartzo-feldspathic matrix with plates of biotite marking the schistosity. The mica content, typically biotite, varies from about 10% to an exceptional 90% in an infolded schist in marble at Hollingworth Cliffs.

Quartz is mostly in mosaic form, either as the matrix or in lenses. Most crystals are strained with sutured margins, although in the thin section of specimen Z.663.4 from Meade Nunatak there are some triple-point junctions between straight-edged quartz crystals. This thin section also shows elongate quartz crystals.

The feldspars take two major forms: as part of the granoblastic matrix with quartz and as single crystals or groups of crystals surrounded wholly or in part by mosaics of strained quartz. The thin section of specimen Z.601.3 demonstrates the latter form where the feldspar (fairly fresh twinned andesine (An_{35}) and heavily sericitized untwinned feldspar with interstitial flakes of sericite, brown biotite and chlorite) is bordered by fine and coarse quartz mosaics of severely strained crystals. In general, the feldspar is difficult to determine either due to the lack of twinning or to the extent of sericitization. However, potash feldspar appears to be absent (no microcline was observed) unless the more heavily sericitized crystals are untwinned orthoclase or microcline.

Biotite is commonly dark brown but the thin section of specimen Z.588.6 from Hollingworth Cliffs contains a pale green-brown mica which has been identified as phlogopite. Crystals are frequently large (5 mm or more in length or diameter) but some schists comprise countless small flakes (about 25 μm or less) which resemble brown "sericite". Zircon inclusions with pleochroic haloes are common.

Specimen Z.588.6 from Hollingworth Cliffs contains phlogopite with accessory muscovite. The thin section has a peculiar texture of intergrown basal plates of phlogopite (i.e. no cleavage visible and a centred interference figure) up to 2 mm long by 0.6 mm broad; $2V\alpha$ is estimated at 5°. The margins of the plates are fuzzy and appear to merge with one another. Normal muscovite plates are also present but similarly fuzzy crystals with a very low birefringence and $2V\alpha$ estimated at 30° are presumed to be basal plates of muscovite. Prehnite also occurs in this thin section.

Epidote occurs as small crystals distributed through the specimens and in the thin section of specimen Z.663.4 (Meade Nunatak) a slip cleavage is marked by extensive epidotization as large (0.5 mm) crystals of yellow pistacite. Accessory minerals include brown sphene in small anhedral crystals with some calcite and sericite, and rare ilmenite.

Garnet-mica-schists

The majority of these schists are very similar to the mica-schists except for the addition of pink garnet. The matrix of the rocks is quartzo-feldspathic with slightly greater proportions of twinned plagioclase of andesine composition, and muscovite is commoner.

Most of the garnets contain inclusions but few show any rotation. In the thin section of specimen Z.829.2 (north-west end of Wedge Ridge), the garnets are syntectonic and contain sinusoidal trains of quartz inclusions indicating about 60° clockwise rotation. This thin section is finely crystalline except for a large quartzite fragment; kink bands are common and a long narrow quartz lens is recumbently folded parallel to the schistosity. In the thin section of specimen Z.585.4 (Jamieson Ridge), the garnets have cores with sinusoidal trains of quartz inclusions surrounded by an inclusion-free zone with an outer zone of spiral trains of quartz inclusions, indicating two periods of rotation and growth separated by a period of growth only. This thin section is also peppered by minute ilmenite crystals.

Two varieties of "classic" garnet-mica-schist occur in the Shackleton Range with limited outcrop but with a wide distribution. Both are best exposed in the Herbert Mountains, where a golden garnet-biotite-schist (Z.585.8) crops out on Jamieson Ridge and a silvery garnet-muscovite-schist (Z.710.2) crops out at the north-west end of the ridge west of McLaren Monolith. In the thin section of specimen Z.585.8 (Fig. 3c), the schistosity, marked by plates of biotite, muscovite and chlorite, is wrapped around large (up to 1 cm in diameter) garnets with inclusions of quartz, ilmenite and muscovite, and fractures parallel to the schistosity infilled with green chlorite. The matrix is essentially mica or chlorite with porphyroblastic epidote and minor amounts of ilmenite. In one part of the thin section a small veinlet or lens of probable pericline shows typical variable extinction and optic axial angle (MacKenzie, 1957). By contrast, in specimen Z.710.2 muscovite predominates over biotite and hence over chlorite, and the rock is finer-grained with smaller garnets (up to 5 mm in diameter). Quartz forms a coarse mosaic with included muscovite plates; epidote and feldspar are absent but around one garnet there is a little fibrous sillimanite and some staurolite.

Kyanite- and staurolite-schists

These schists have been found only at Lewis Chain, Lord Nunatak and M'Clintock Bastion. In most specimens, both minerals occur in what is otherwise a garnet-mica-schist. The schistosity is marked by bands of mica (muscovite and/or biotite) with equant or elongate quartz crystals wrapped around garnets, and lenses of quartz or oligoclase (about An_{28}) mosaic. Kyanite occurs as typical bladed crystals generally parallel to the schistosity, whereas staurolite forms large (up to 5 mm in diameter) irregular yellow crystals with innumerable inclusions of quartz and muscovite (Fig. 3d) and is usually associated with garnet. The garnets (up to 7 mm in diameter) also contain quartz inclusions but show no evidence of rotation. In the thin section of specimen Z.657.1 (Lord Nunatak), there are some accessory brown tourmaline crystals with green cores, presumably zoned schorlite. These crystals show centred uniaxial interference figures, indicating parallel alignment within the schistosity and they probably represent original detrital grains. In the thin section of specimen Z.669.7 (southern nunatak of the Lewis Chain), staurolite is absent and kyanite is present in small quantities only, probably due to a lower alumina content of the original rock.

Sillimanite-schists

So far, only one specimen has been found containing sillimanite in any quantity. This rock (Z.686.2), from the northern part of Hatch Plain, is a coarse quartzo-feldspathic garnet-mica-schist with a very little interstitial sillimanite. The mica is brown biotite, often altered to colourless chlorite. Much of the feldspar is heavily sericitized but some twinned plagioclase crystals are identifiable as oligoclase (about An_{28}). Most quartz crystals are highly strained and, with feldspar, form a mosaic comprising most of the rock. The sillimanite forms narrow veinlets and small aggregates of laths between sericitized feldspars and is often intimately associated with biotite plates.

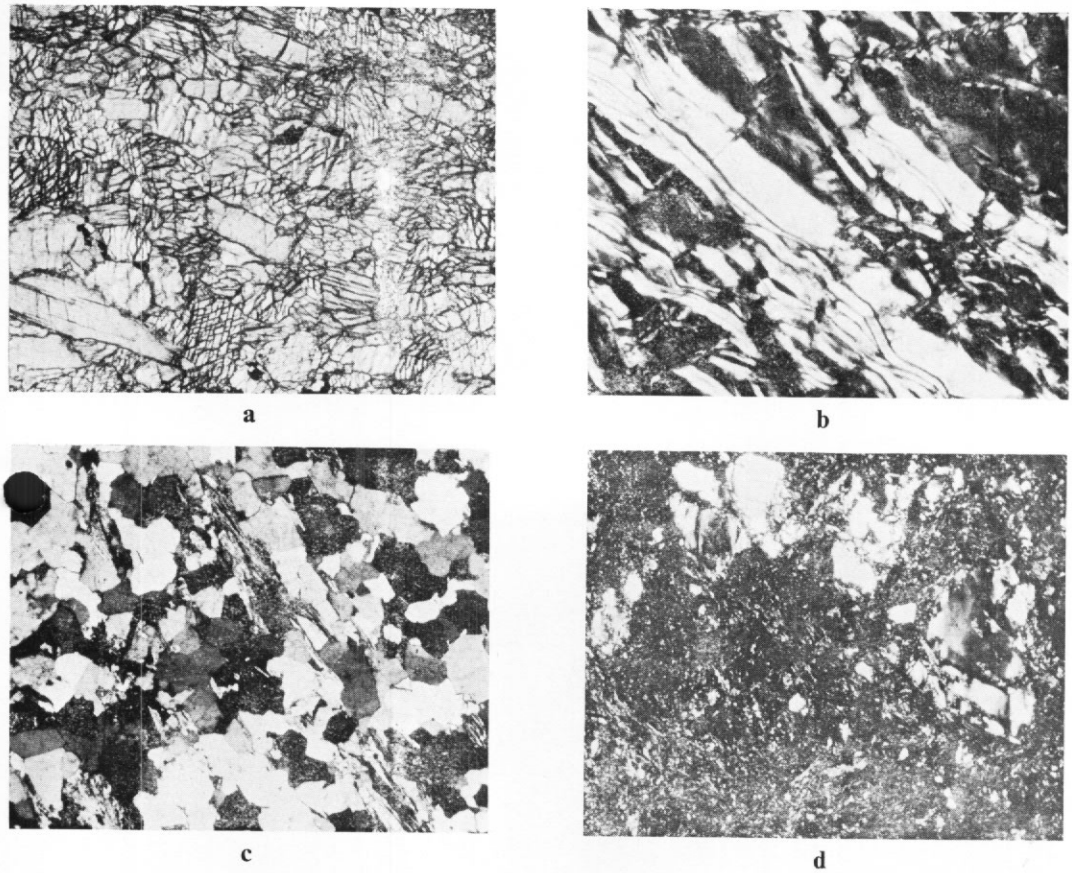

Fig. 6. a. Hornblende crystals in a garnet-amphibolite (Z.708.1; ordinary light; ×27).
b. Replacement of diopside by chrysotile in a diopside-chrysotile-marble (Z.729.2; X-nicols; ×150).
c. Granoblastic quartz matrix with plates of muscovite and chlorite in a quartz-schist (Z.660.2; X-nicols; ×27).
d. Quartz-mylonite with strained quartz in a quartz-sericite-chlorite matrix (Z.599.5; X-nicols; ×29).

pargasite, indicating a magnesium-rich or dolomitic horizon in the original limestone. The thin section of specimen Z.588.5 is about 95% amphibole with minor amounts of interstitial calcite, strained quartz, sphene and muscovite, with some inclusions of epidote (pistacite) in the amphibole.

The field relations of many of the amphibolites suggest a sedimentary origin, from iron- and magnesium-rich limestones, which is not contradicted by the petrography. However, in such a large area as the Shackleton Range, it would be reasonable to expect some basic intrusions and, although no relict igneous textures have been seen, e.g. ophitic texture, some of the amphibolites, particularly those occurring as lenses in gneisses and schists, could well be *ortho*-amphibolites.

Calcareous Rocks

The calcareous rocks may be subdivided into three groups: marbles, found as pods and lenses in gneisses or occurring as large bodies of unknown shape and dimensions, calcareous schists, and metalimestones. None of these rocks shows any regular geographical distribution except that they occur, almost exclusively, in the more northerly parts of the range.

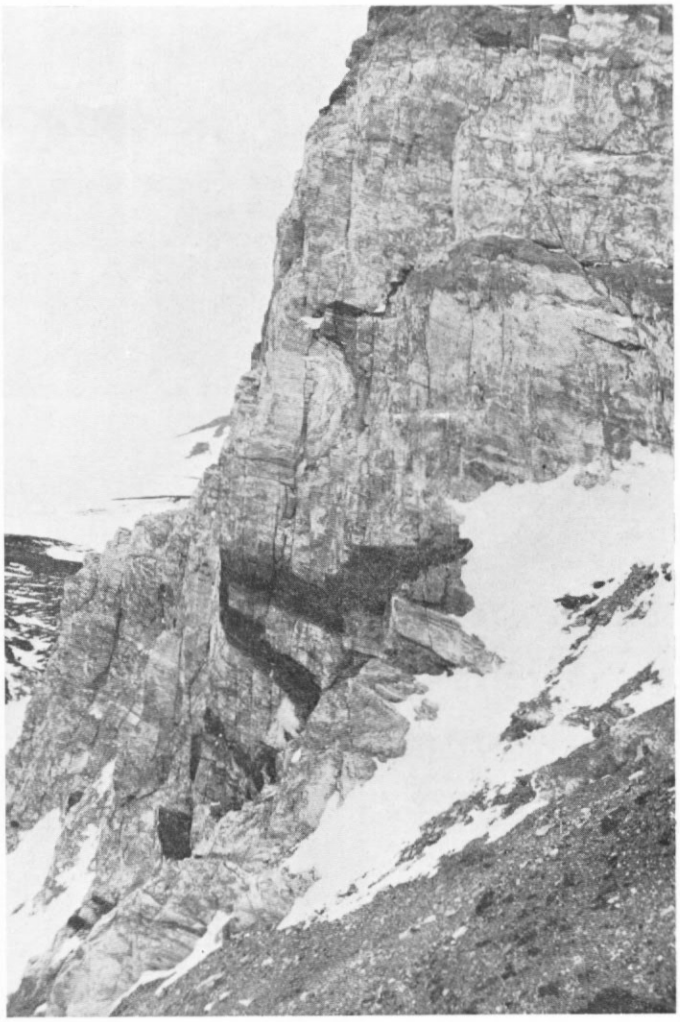

Fig. 7. Massive marbles with infolded mica- and amphibole-rich bands forming Hollingworth Cliffs in the south-eastern Herbert Mountains.

Marbles

The largest outcrop of marble, a diopside-chrysotile-marble, forms Hollingworth Cliffs (Fig. 7). In the thin section of specimen Z.588.1 the calcite is completely recrystallized to a coarse mosaic (up to 1 mm in diameter) and forms 70–80%, some crystals showing deformation twin lamellae. The pyroxene occurs as small crystals (about 0.3 mm in diameter), which are often parts of larger crystals now altered to fibrous chrysotile. The chrysotile forms bands parallel to the pyroxene boundaries with the fibres at right-angles. The pyroxene is difficult to identify but it is probably diopside.

On the lower slopes of the ridge (Z.729) 4.5 km west of Mount Etchells, a pod of marble several metres wide is essentially similar to that at Hollingworth Cliffs but it is much smaller. Massive green chrysotile is a prominent feature in the hand specimen and the thin section (Z.729.2) shows extensive areas of chrysotile replacing pyroxene (again presumed to be diopside) along cleavages and fractures (Fig. 6b). Calcite is virtually absent from the thin

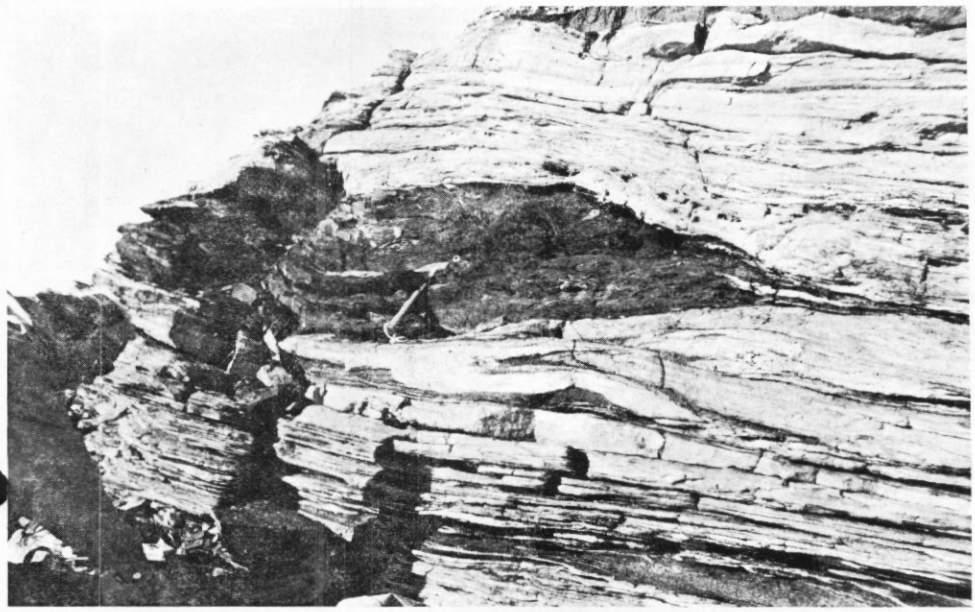

Fig. 4. Amphibolite lens in hornblende-schist near the summit of Charpentier Pyramid in the Herbert Mountains.

Chlorite-schists

Although chlorite is common as an alteration product of other silicates, notably biotite, it rarely forms a distinct rock type. However, specimen Z.587.2 (Ramsay Wedge) is from a band of chlorite-actinolite-schist. About 30% of the thin section is composed of plates and radiating aggregates of pleochroic green to pale green or colourless, optically negative penninite with wavy extinction and anomalous green-grey birefringence. Muscovite is often interleaved with chlorite but large areas of the latter exist and it appears to be a primary mineral. There are a few laths (up to 7.5 mm long) of pale green actinolite which have deformed and grown through muscovite plates. Large plagioclase porphyroblasts (up to 4 mm in diameter) are zoned and sericitized but untwinned. Accessory minerals include ilmenite, haematite and probably brown sphene but no quartz. This rock represents the greenschist facies, probably the quartz-albite-muscovite-chlorite sub-facies (Turner and Verhoogen, 1960).

Amphibolites

Amphibolites have two principal modes of occurrence: most commonly they form bands and lenses within gneisses and schists from about 1 m to tens of metres in length (Fig. 4), and secondly as continuous horizons a few metres thick interstratified with metalimestones. The lenses are common throughout the range, whereas the continuous horizons are largely restricted to the central parts of the Haskard Highlands, the Lagrange Nunataks and the Herbert Mountains.

The largest amphibolite found in the range forms much of the ridge extending south from Sumgin Buttress (Fig. 5). It is about 300 m thick, dipping gently eastward, and comprises massive amphibolites with garnetiferous horizons. This thick uninterrupted sequence of amphibolite has not been found elsewhere in the range.

In thin section this amphibolite is composed of up to 90% hornblende, pleochroic from dark green to pale brown, forming a mosaic of anhedral to subhedral crystals (0.5–1.0 mm

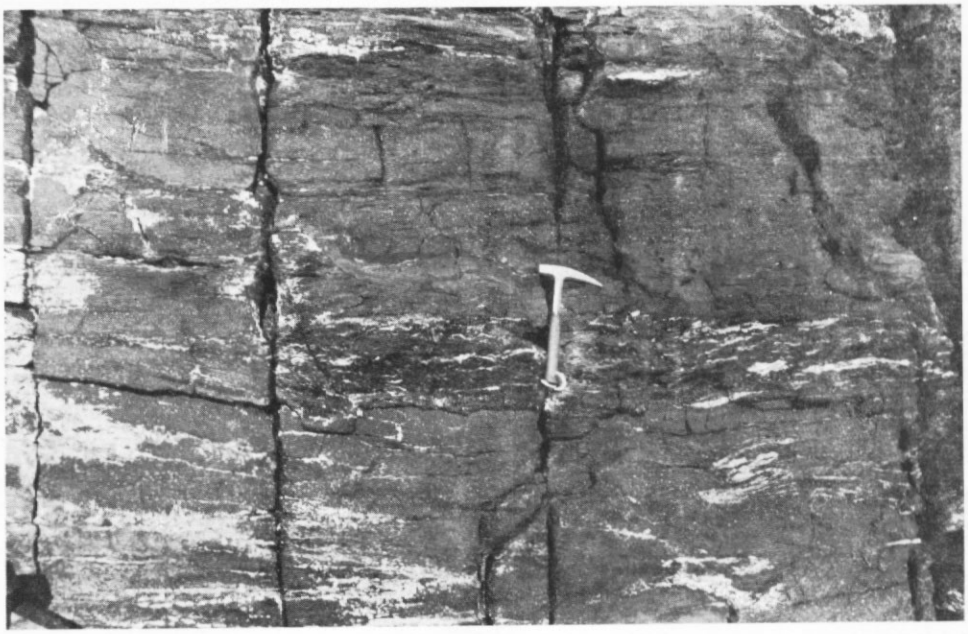

Fig. 5. Garnet-amphibolite at station Z.945 on the ridge south of Sumgin Buttress in the Herbert Mountains.

in diameter) with some inclusions of quartz which are occasionally "euhedral pseudomorphs" controlled by amphibole cleavage directions. Accessory minerals occurring interstitially include quartz, zircon (which may form pleochroic haloes), untwinned and twinned, sericitized and fresh plagioclase, garnet, ilmenite, rare ilmeno-haematite and much calcite. Other thin sections from this amphibolite (Fig. 6a) show a good foliation which is demonstrated by laths of hornblende and some of pale green actinolite, and severely strained quartz crystals (Z.946.1). Zoning in the hornblendes is not uncommon and one particular crystal has a pale blue-green core with a broad pale green rim, both pleochroic to paler colours. No relict igneous textures were observed so the pre-metamorphic rock type is uncertain.

The amphibolites of discontinuous bands and lenses are essentially similar to those described above, although the amphibole content is not always so high. Specimen Z.601.8 is coarser (crystals about 2 mm in diameter) and the hornblende is pleochroic from pale brown to very pale brown with pale blue-green rims in optical continuity. Plagioclase, interstitial to hornblende, is generally sericitized and untwinned, although rare twinned crystals are optically positive with low twin angles indicating an albite/oligoclase composition. Quartz occurs as inclusions in hornblende and also in the groundmass which is largely sericite or sericitized plagioclase. Ilmenite is present as an accessory mineral.

An amphibolite from Watts Needle, in the south-west Read Mountains (Z.593.3), is associated with pale grey limestones. It comprises about 50% hornblende crystals 1–2 mm in length which are pleochroic from green-brown to pale brown with frequent chloritization along cleavages and fractures. Plagioclase, probably albite or oligoclase, is heavily sericitized, untwinned or poorly twinned and constitutes most of the remainder of the thin section. Accessory minerals include chlorite, some interstitial calcite and rare ilmenite. No relict textures were seen to indicate the original rock type but the association of the amphibolite with metalimestone suggests that the amphibolite represents a metamorphosed iron- and magnesium-rich limestone.

The infolded amphibolites in the marble buttresses of Hollingworth Cliffs contain pale blue-green, barely pleochroic amphiboles which are optically positive and hence, are probably

section except as replacement veins in pyroxene. There are some small crystals of colourless, anomalously blue and brown-grey birefringent clinochlore between areas of calcite and chrysotile. The blue birefringent crystals sometimes form on the ends of squat, brown-grey birefringent crystals, suggesting a later origin of the former. The earlier crystals may have formed after mica on account of their speckled or mottled appearance either side of the extinction position.

Calcareous schists

Calcareous schists occur in many parts of the range and are not necessarily associated with either marbles or metalimestones, although they are often found with amphibolites. It seems likely that many of the outcrops along Pioneers Escarpment may be formed of calcareous schists.

In thin section these rocks consist of completely recrystallized calcite mosaic enclosing accessory quartz, opaque and micaceous minerals which mark the schistosity. About 70% of specimen Z.655.1 (Lord Nunatak) is a calcite mosaic enclosing sub-angular to rounded, slightly strained quartz crystals and quartzite fragments. The undulating schistosity is marked by orientated muscovite plates and associated trains of small ilmenite crystals. Some ilmenite occurs as a dense aggregate of inclusions in an unidentified host mineral, possibly plagioclase. Other anhedral to euhedral opaque crystals distributed across the thin section appear to be pyrite or pyrrhotite which has been partially oxidized to haematite. The origin of the quartzite fragments is uncertain; it may be brecciated vein quartz or detrital quartzite in an originally impure limestone. Colourless brown-grey birefringent chlorite, possibly clinochlore, may be altered biotite.

On the southern nunatak of Lewis Chain (Z.669), calcareous schists are interbedded with metalimestones. These schists are generally banded, layers of calcite mosaic alternating between micaceous layers with quartz lenses. The calcite layers are generally fairly pure with inclusions of quartz and sub-angular to rounded intergranular crystals of quartz or fragments of quartzite; orientated plates of brown biotite, muscovite, colourless or neutral chlorite and rare epidote also occur. The micaceous layers are composed of biotite and chlorite in a matrix of sericite with minor amounts of muscovite, plagioclase, parallel and elongated calcite crystals and some quartz. Quartz lenses are formed of a mosaic of strained quartz crystals with thin plates of biotite and some calcite.

Metalimestones

The metalimestones are pale blue-grey finely crystalline rocks which may be massive or well-bedded, compact or friable. The main occurrences are between Williams Ridge and Mount Peters, south-east of Butterfly Knoll, at the southern nunatak of Lewis Chain and at the southern end of Bernhardi Heights.

At the outcrop south-east of Butterfly Knoll (Z.732), the rock varies from about 95% recrystallized calcite mosaic (grain-size about 0.2 mm) with anhedral rhombs and fibres of tremolite (Z.732.2) to an impure limestone of about 50% calcite mosaic with anhedral quartz crystals, fragments of quartzite and crystals and fibres of tremolite embayed by calcite. Specimen Z.669.2, from the southern nunatak of Lewis Chain (Fig. 8), is 99% recrystallized calcite with traces of muscovite and quartz crystals, whereas specimen Z.669.4 is a fine-grained (crystals about 0.1 mm in diameter) calcite mosaic with tremolite fibres up to 1.5 cm long and parallel plates of muscovite. Specimen Z.711.2, from central Bernhardi Heights, is 99% calcite mosaic with traces of quartz, muscovite and myriad opaque crystals.

Thus the mineralogy of these rocks is essentially similar, although the proportions of the minerals vary considerably. The calcareous schists may represent a similar but less pure limestone facies.

Quartzites

Quartzites and micaceous quartzites or quartz-schists are found throughout the range but they are not very common.

Quartzites

Two types of quartzite have been found in the range: a rock consisting of 98% or more quartz in a granoblastic polygonal network with some crystal elongation and a rock with a mortar texture of larger quartz crystals in a fine-grained matrix of quartz and subordinate feldspar.

The first type has a grain-size of about 1.5 mm and has a thinly schistose or flaggy texture in the hand specimen along planes marked, in thin section, by short narrow parallel plates of muscovite. None of the quartz crystals shows any secondary enlargement, indicating that the whole rock has been recrystallized, and undulose extinction due to strain is universal. Some of these rocks are a distinctive pale green colour in the hand specimen, e.g. Z.665.1 from Sauria Buttress (Fig. 9), which is attributed to fuchsite, a green chromium-bearing variety of muscovite which is colourless in thin section.

The second type with mortar texture is less pure and contains feldspar in the matrix. Specimen Z.593.5 (Watts Needle) consists of large (up to 0.7 mm in diameter) angular to sub-rounded strained quartz crystals; the feldspar crystals are generally smaller and are either twinned plagioclase or perthite. In the thin section of specimen Z.659.2 (Jackson Tooth), the coarser quartz is often in mosaic form rather than in single crystals and the matrix has a recrystallized granoblastic texture with much heavily sericitized untwinned feldspar. There is also a little chlorite and some fibrous laths and scattered crystals of prehnite but no mica.

Fig. 8. Metalimestone at station Z.669 on the southern nunatak of Lewis Chain in the Lagrange Nunataks.

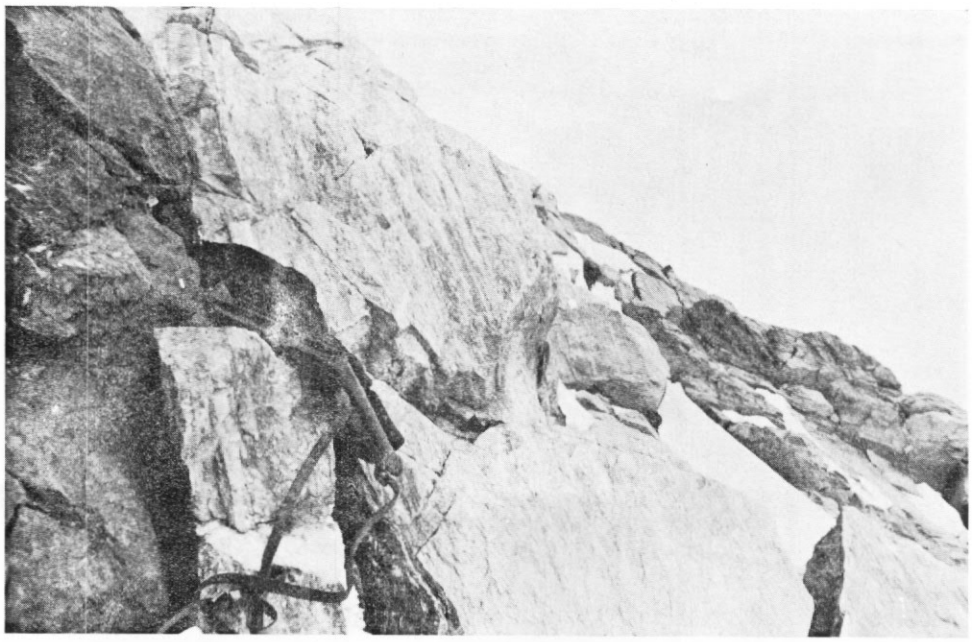

Fig. 9. Steeply dipping hornblende-schist, quartz-schist and quartzite at Sauria Buttress, Pioneers Escarpment.

Quartz-schists

These rocks are very similar to the first type of quartzite (p. 268) but their mica content is higher and in the hand specimen they possess a well-defined schistosity. In the thin section of specimen Z.660.2 from Jackson Tooth (Fig. 6c), the quartz matrix has a granoblastic polygonal texture; individual crystals show little strain and the schistosity is strongly marked by parallelism of muscovite plates, many of which are altered to green penninite. There is some accessory sphene and some ore, probably ilmenite.

Quartz-mylonite

Thrust contacts between rocks often produce mylonitization but only one major mylonite has been observed by the author in the Shackleton Range. At the northern end of the ridge between Glen Glacier and Kuno Cirque (Z.599), a quartz-mylonite about 1 m thick separates augen-gneiss to the west from migmatites to the east (Fig. 10). In the thin section of specimen Z.599.5 the rock is composed of shattered and strained quartz and heavily sericitized feldspar porphyroclasts (up to 0.7 mm in diameter) in a microcrystalline groundmass of quartz, sericite and some feldspar (Fig. 6d). Pale green chlorite has pervaded the groundmass and also forms long thin stringlets generally sub-parallel except where they are "folded" by internal shearing forces. Porphyroclastic ilmenite is rimmed with leucoxene which is also common in stringlets like the chlorite.

Migmatites

Migmatites are exposed throughout the Shackleton Range but they reach their maximum development in the Read Mountains, culminating in the intrusion of granite and granodiorite. In the Read Mountains almost all of the rocks have been migmatized to some degree, whereas in other parts of the range the lower-grade and more calcareous metamorphic rocks are

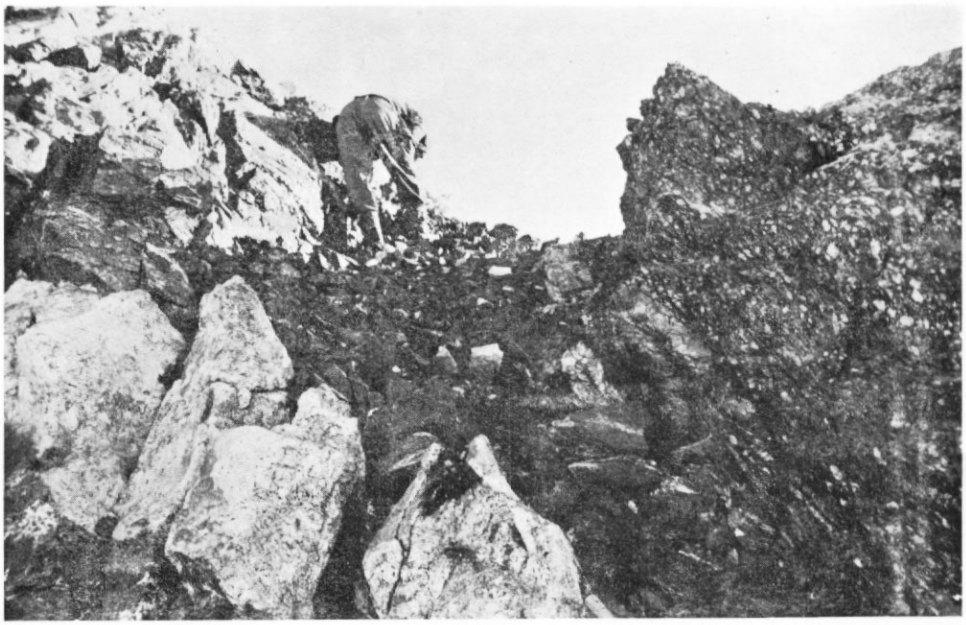

Fig. 10. Quartz-mylonite occupying a thrust zone which separates migmatite from augen-gneiss at station Z.599 between Glen Glacier and Kuno Cirque in the western Read Mountains.

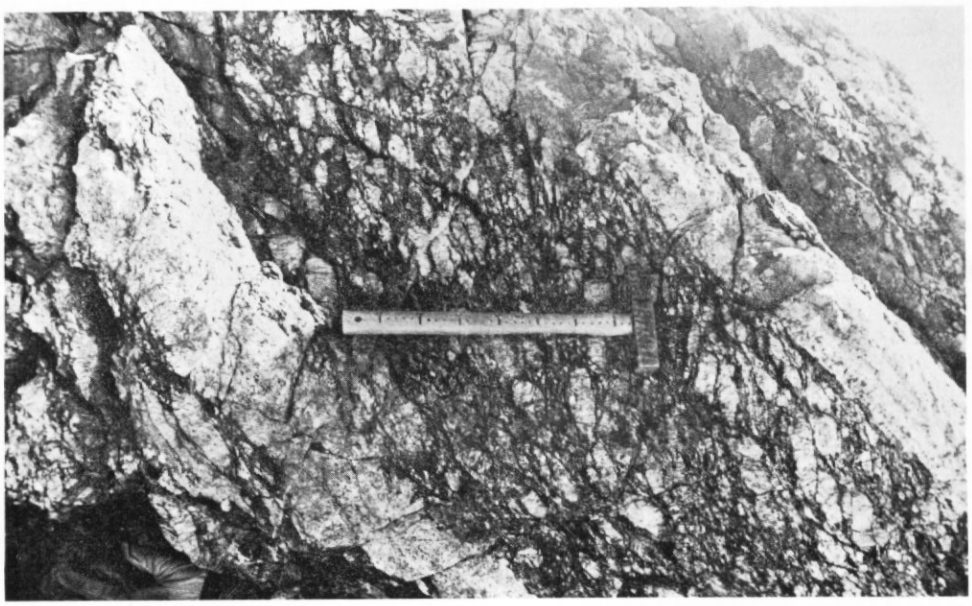

Fig. 11. Augen-gneiss cut by granitic veins at station Z.599 between Glen Glacier and Kuno Cirque in the western Read Mountains.

commoner or predominate, particularly in the Herbert Mountains. In these other areas, unexposed contacts between migmatite outcrops and the surrounding country rocks are presumed to be fault or thrust planes.

Field relations

The migmatite neosomes take several forms, ranging from augen-gneiss to granite pluton. The augen-gneisses are considered to have resulted from the metasomatism of basic country-rock gneisses (Fig. 11) because the feldspar porphyroblasts do not appear to be directly related to the acid veins which frequently cut these rocks. The agmatitic neosomes are probably the commonest type (Clarkson, 1972, fig. 2) and are apparently intrusive in origin. In some examples, pegmatitic margins to one side of a neosome may have been caused by the upward streaming of volatiles and therefore may indicate the orientation of the rock at the time of crystallization.

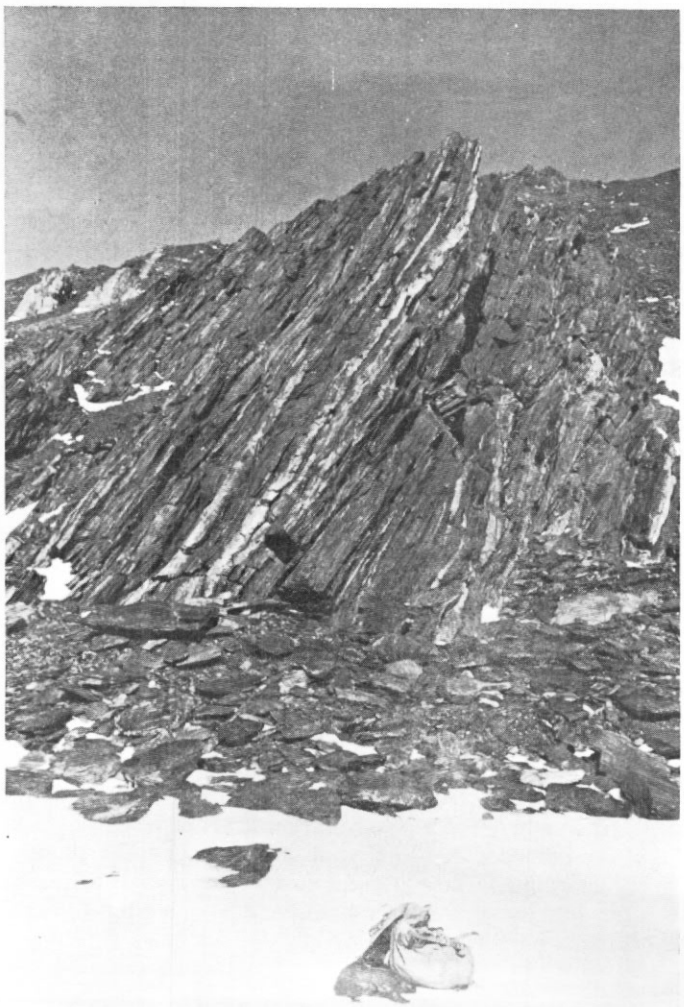

Fig. 12. *Lit-par-lit* migmatization of a basic gneiss palaeosome by granitic neosomes at station Z.864, 3 km north of The Ark in the western Read Mountains.

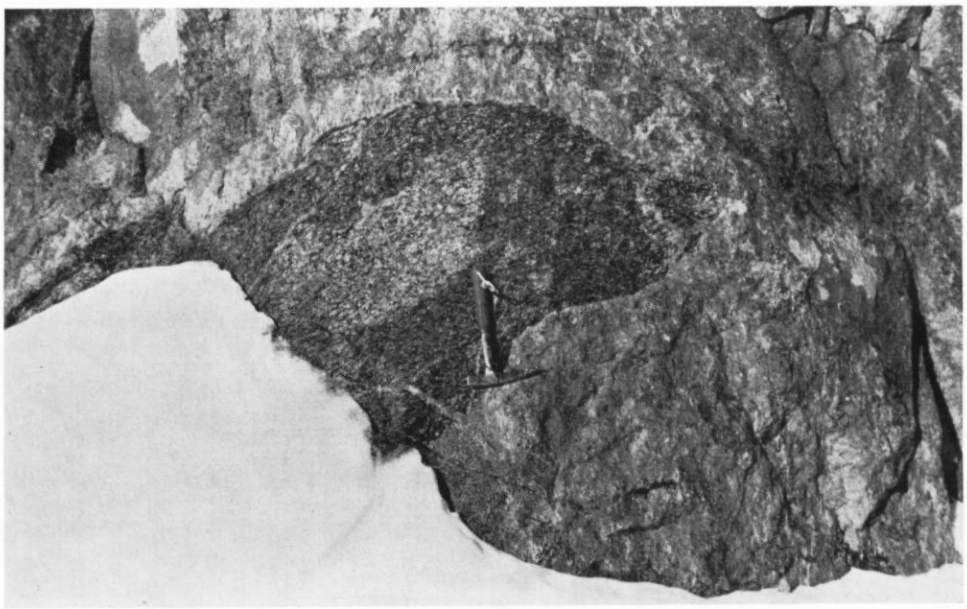

Fig. 13. Xenolith of basic gneiss in a large granitic neosome at station Z.870 at the foot of the escarpment below Holmes Summit in the western Read Mountains.

The most obvious examples of intrusive neosomes are the regular parallel-sided veins up to 4 m or more wide. They show either cross-cutting dyke relations to the structure of the palaeosome or *lit-par-lit* intrusion (Fig. 12) which may have suffered subsequent boundinage. Some acid dykes have narrow chilled margins, implying that they are probably later than the agmatites at the same level because of the relatively mobile or plastic state of the palaeosome during the intrusion of the latter. The largest of the acid veins are irregular in shape but their intrusive origin is shown by the presence of xenoliths of more basic gneiss with a reaction rim against a chilled margin to the granitic host (Fig. 13). These granite veins reach their ultimate development in the granite plutons where different phases of intrusion can often be recognized, although the plutons appear to be homogeneous at first sight (Fig. 14).

The final event of the migmatization episode was the intrusion of the granodiorite dyke exposed in the south face of Hatch Plain. The margins of the dyke are slightly chilled against the host granite but not enough to suggest that the time of intrusion was significantly different from the time of emplacement of the granite. The dyke has been dated at 1 446±60 M[illegible] (Rex, 1971) and thus provides a minimum age for migmatization. At present this is the only age available to indicate the time of the metamorphic events in the basement complex.

The isolation of many outcrops and the non-continuous exposure of others has precluded attempts to zone the migmatites. It is fairly clear that migmatites predominate along the southern parts of the range where the basement complex is exposed but, apart from a general observation that the parallel-sided neosomes are more frequent in the area of the plutons, no zonation has been determined. Any original pattern of migmatization has doubtless been complicated by tectonic activity such as has already been suggested to explain the migmatite distribution in the northern parts of the range.

Petrography

The country-rock gneisses, which form the palaeosome of the migmatites, are mostly dioritic or quartz-dioritic in composition. They are dark-coloured and well foliated with

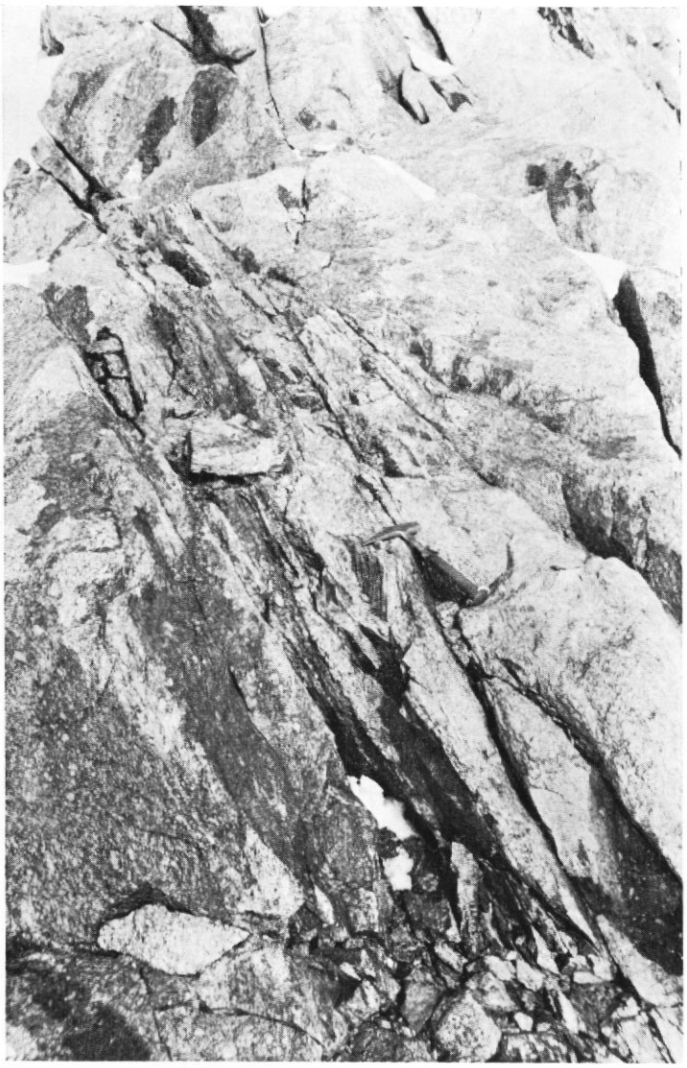

14. Granite at station Z.860 along the ridge between The Ark and Watts Needle in the western Read Mountains.

substantial proportions of hornblende and/or biotite. Plagioclase is the dominant feldspar but perthitic types and heavily sericitized untwinned feldspars make accurate composition determinations difficult. Accessory minerals include sphene, epidote, chlorite, garnet, zircon and iron ore.

In thin section the grain-size is often comparatively fine, rarely more than 5 mm in diameter and the foliation is not always well marked. Quartz occurs as clear equant grains or as a recrystallized mosaic; strain, shown by undulose extinction, is common, particularly in mosaic lenses. Rounded quartz grains are common in feldspar porphyroblasts.

Feldspar is probably commonest as very heavily sericitized crystals so that determination is difficult or impossible. In specimen Z.707.1 (MacLaren Monolith), the feldspar is remarkably fresh with well-twinned andesine crystals (about An_{39}), optically positive untwinned feldspar

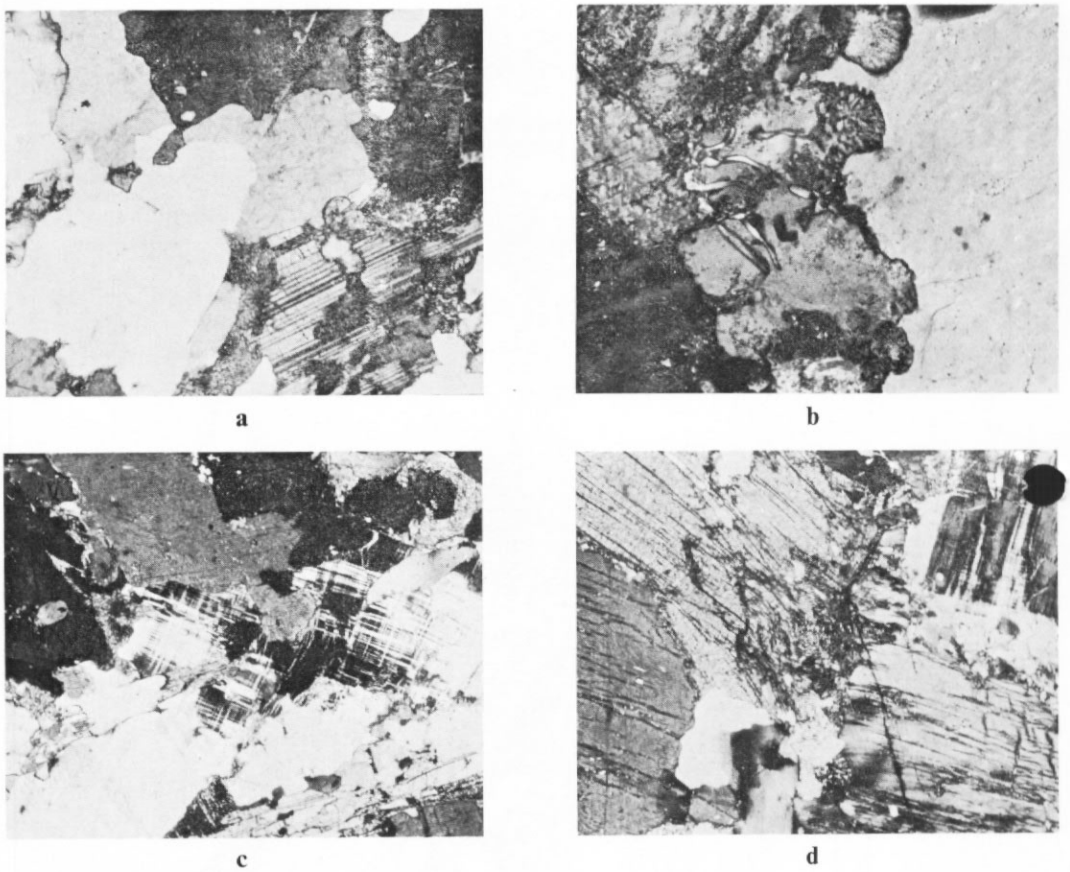

Fig. 15. a. Quartz, biotite, andesine and untwinned feldspar in a dioritic gneiss (Z.707.1; X-nicols; ×27).
b. Myrmekite between microcline-microperthite and oligoclase with biotite, untwinned feldspar and quartz in an augen-gneiss (Z.594.5; X-nicols; ×110).
c. Hornblende, quartz, microcline, biotite and plagioclase in a granitic neosome (Z.603.1; X-nicols; ×27).
d. Large perthitic feldspars, biotite, quartz and microcline in a granite (Z.691.1; X-nicols; ×75).

with its refractive index approximately equal to that of balsam (probably albite) and some perthitic feldspar (Fig. 15a). The perthitic feldspar is a patch or braid type (Spry, 1969, p. 18[illegible] the two components providing separate extinction positions but both being optically positive, possibly a peristerite structure (Deer and others, 1966). Antiperthitic andesine porphyroblasts contain patches of microcline with characteristic "tartan" twinning, although they are apparently optically positive. One crystal of microcline with poorly developed "tartan" twinning and refractive indices less than balsam is also apparently optically positive. Quartz and biotite inclusions are common and some crystals contain calcite veinlets and blebs. In many thin sections the feldspars are perthitic but, as neither the host nor the enclosed feldspars are twinned, it is not possible to ascertain whether the feldspar is perthite or antiperthite.

Biotite is the principal mica in these gneisses. It is commonly pleochroic from dark brown to pale brown, although green varieties occur and many plates are partly altered to chlorite. Where hornblende is also present, the two minerals often form adjacent parallel crystals.

Hornblende generally has the pleochroism scheme α = pale brown, β = green, γ = dark

blue-green. In specimen Z.728.8 (Mount Etchells), the hornblende is largely turbid with countless minute inclusions, particularly concentrated along thin transverse fractures and the crystals are rimmed with a pale blue-green amphibole.

Specimen Z.685.1 is a pyroxene-gneiss with crystals of augite up to 9 mm in diameter forming about 70% of the thin section. This rock appears to belong to the pyroxene-granulite facies but the presence of small sphene crystals must refer it to the lower-grade hornblende-granulite facies (Turner and Verhoogen, 1960).

Pale pink garnets occur in some rocks, although porphyroblasts up to 5 cm in diameter are known (Stephenson, 1966). Garnet is not very common in the thin sections examined but it is found as porphyroblasts in mafic bands (Z.712.1; Bernhardi Heights) or less commonly as inclusions in feldspar (Z.723.2; Morris Hills).

Accessory minerals include rare muscovite and some equant crystals of epidote; chlorite is often present as an alteration product of biotite and garnet, and zircon and calcite also occur. Ilmenite is the principal ore mineral, often with a rim of haematite and sometimes surrounded by sphene.

In addition to the dioritic gneisses described above, there are some granitic gneisses. These are interstratified with the more basic gneisses but are paler in colour, frequently massive and not as well foliated. In thin section their mineralogy is similar to that of the dioritic gneisses but they contain more quartz and feldspar and less hornblende and biotite. Plagioclase is very heavily sericitized and fractures are filled with sericite, chlorite or, rarely, calcite. Accessory minerals include zircon, rare garnet and ore minerals, typically ilmenite.

The augen-gneisses are dark, massive medium-grained gneisses with feldspar porphyroblasts up to 16 cm long. They usually possess a coarse foliation shown by the alignment of the major axes of the feldspar augen. The augen-gneisses are frequently cut by granitic migmatite neosomes (Fig. 11).

The feldspar porphyroblasts are usually microcline-microperthite, which may include crystals of quartz, biotite and other rarely sericitized feldspars. The matrix contains similar microperthite, oligoclase which is frequently sericitized and untwinned plagioclase or possibly cryptoperthite. Myrmekite is common (Fig. 15b). Quartz is present in patches of mosaic; individual crystals are strained with sutured common margins but smooth margins against feldspars.

Dark brown biotite, rarely altered to chlorite, is normally the only mica present and the plates show no preferred orientation. A colourless, neutral or straw-yellow amphibole, slightly pleochroic and sometimes fibrous (possibly actinolite), occurs as a minor constituent in some thin sections. It is usually rimmed by a pale green amphibole, possibly uralite developed during metasomatism, and it is associated with biotite-rich bands. Accessory minerals are rare but they include garnet, epidote, calcite, haematite and ilmenite.

The migmatite neosomes and the granite plutons are petrologically very similar; both comprise microcline, perthite and plagioclase feldspars with quartz, biotite and some hornblende (Fig. 15c). The major difference between the two types in the hand specimen is the grain-size; the plutonic granite is much coarser than the neosomes, although the latter occasionally exhibit pegmatitic phases.

The granite of Hatch Plain is composed of microcline, microcline-perthite, heavily sericitized plagioclase (probably oligoclase) and mosaics of strained quartz with interstitial myrmekite and brown biotite. In the thin section of specimen Z.691.1 (Fig. 15d), the brown biotite is extensively altered to chlorite and many crystals are rimmed with finely granular epidote. The granite forming part of the ridge between The Ark and Watts Needle is similar to that at Hatch Plain but it appears to contain more quartz and less microcline. Specimens from station Z.860 (Fig. 14) show evidence of shearing with feldspars up to 5 mm in diameter set in a matrix of fine-grained quartz mosaic with streaked and elongated crystals. These shearing effects may be due to successive intrusion phases of the granite.

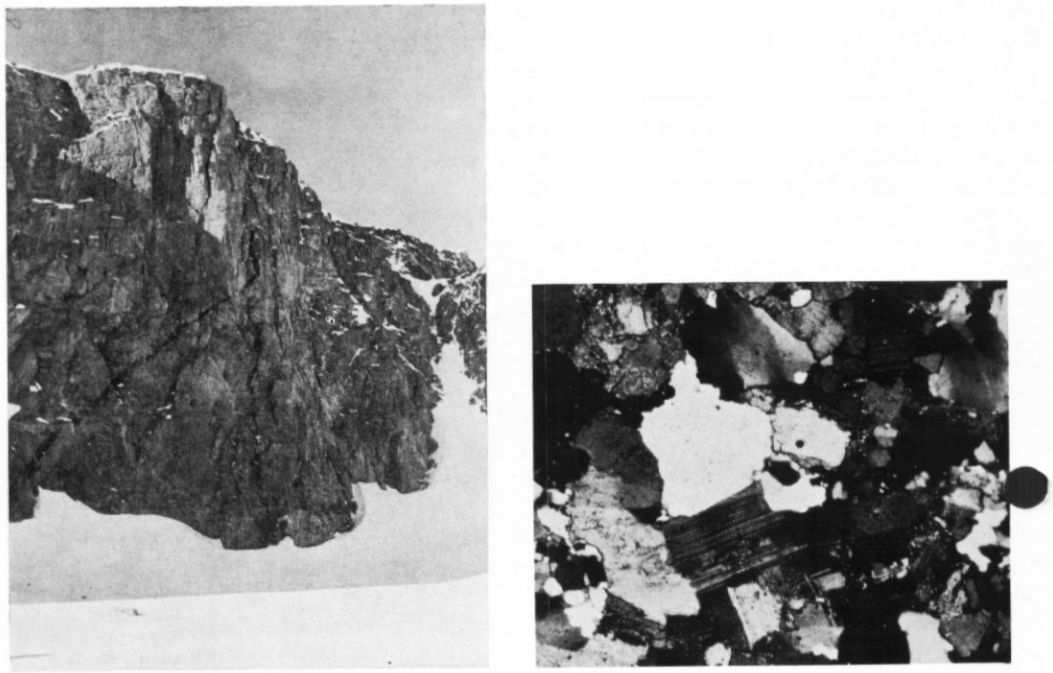

a b

Fig. 16. a. A granodiorite dyke intruding granite in the south face of Hatch Plain, Dutoit Nunataks. (Photograph by M. J. Skidmore.)
b. Quartz, andesine, biotite and hornblende in a granodiorite dyke (Z.602.2; X-nicols; ×27).

The migmatite neosomes are petrographically similar to the granite plutons; the thin section of specimen Z.601.1, from the nunataks at the north-west corner of Glen Glacier, is typical of these rocks. Large porphyroblasts (up to 1.5 cm across) of microcline and microcline-perthite and smaller (up to 5 mm across) crystals of heavily sericitized plagioclase and untwinned feldspar are bordered and cut by areas and veinlets of recrystallized and strained quartz mosaic. Straining of feldspars is indicated by distortion of twin lamellae, by apparent lateral displacement of twin lamellae across quartz veinlets and by occasional marginal granulation of crystals. Myrmekite is absent from this thin section; green chlorite and rare sphene are the only accessory minerals.

The single dyke of granodiorite intruding the granite in the south face of Hatch Pl[illegible] (Fig. 16a) is about 2.5 m wide at the base of the cliff and thins upward and eastward; the plane of intrusion is approximately north–south. In the thin section of specimen Z.602.2 (Fig. 16b), the rock comprises quartz, feldspar, biotite and ore. Quartz is present as clear strained crystals (up to 0.4 mm in diameter) often in patches of mosaic. Plagioclase (about An_{32}) is predominant over untwinned (?) albite or cryptoperthite and rare microcline. The feldspars are comparatively fresh except for the untwinned varieties which are frequently heavily sericitized; crystals are up to 1.5 mm in diameter. Biotite occurs as short plates, pleochroic from dark brown to very pale brown, and as uniformly brown basal plates; there is no preferred orientation. It is usually interstitial to quartz and feldspar, although some plates are included in feldspar. Hornblende, pleochroic from green to very pale green, has a similar form and habit to biotite with which it is often associated. The very small opaque crystals are probably ilmenite. The margin of the dyke is poorly marked in thin section but it may be recognized by the change from biotite in the dyke to chloritized biotite in the granite.

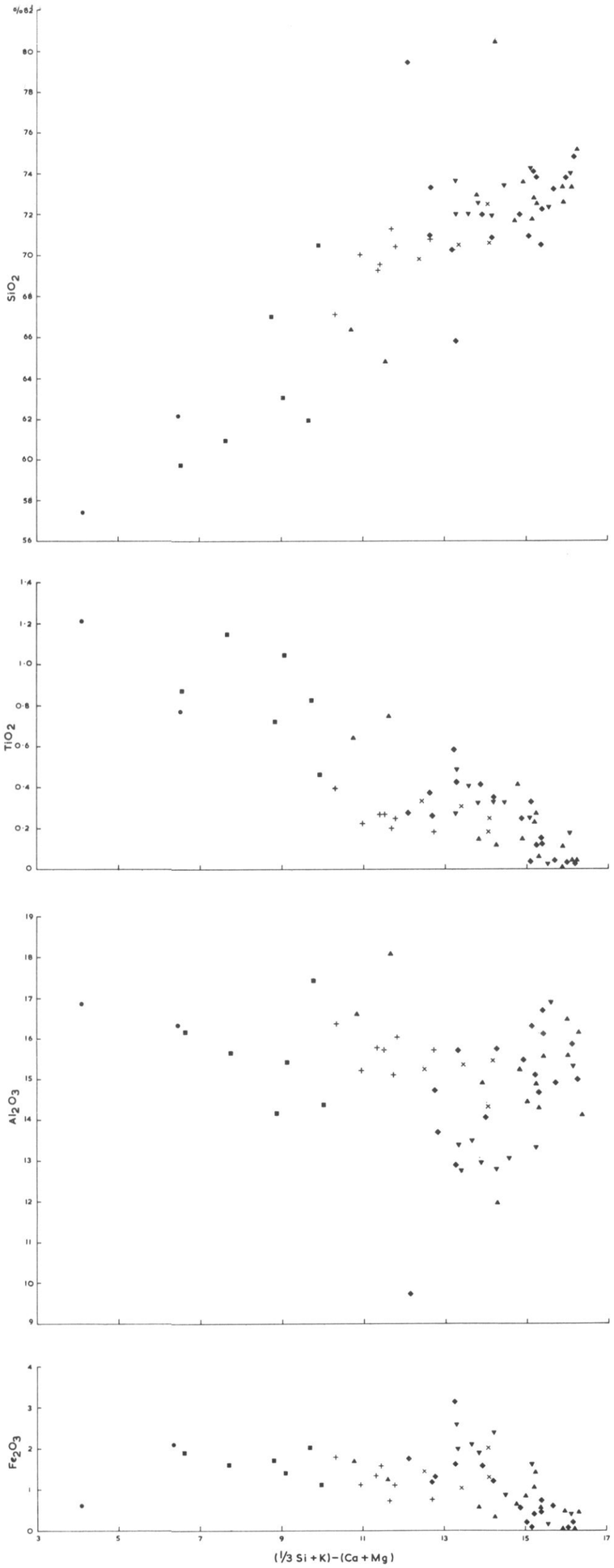

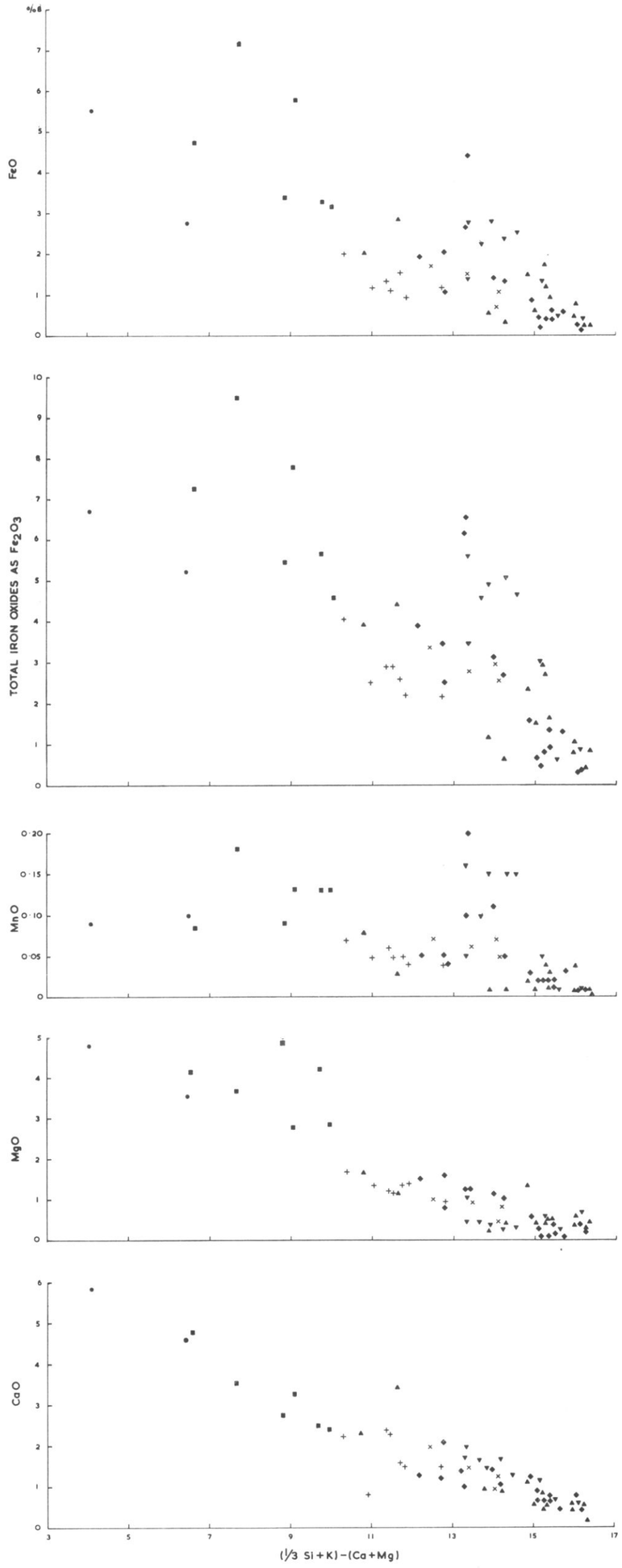

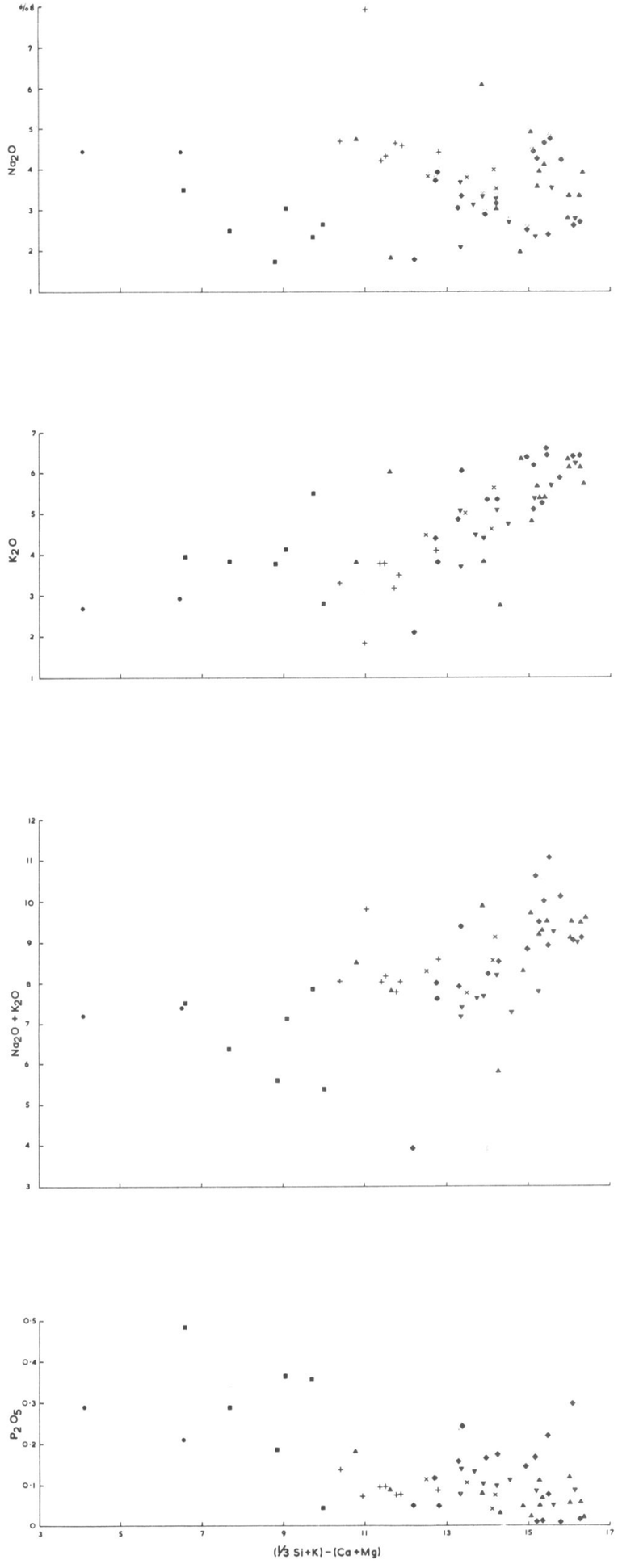

Fig. 17. Plots of major oxides (recalculated to 100% anhydrous) for analyses of granodiorite, augen-gneiss, granite and migmatite neosomes against the modified Larsen index (after Nockolds and Allen, 1953).
- ● Granodiorite dyke.
- ■ Augen-gneisses.
- × Granite (The Ark to Watts Needle).
- \+ Granite (Hatch Plain).
- ◆ Migmatite neosomes (Read Mountains).
- ▲ Migmatite neosomes (Otter and Haskard Highlands).
- ▼ Migmatite neosomes (Herbert Mountains and Lagrange Nunataks).

face page 276

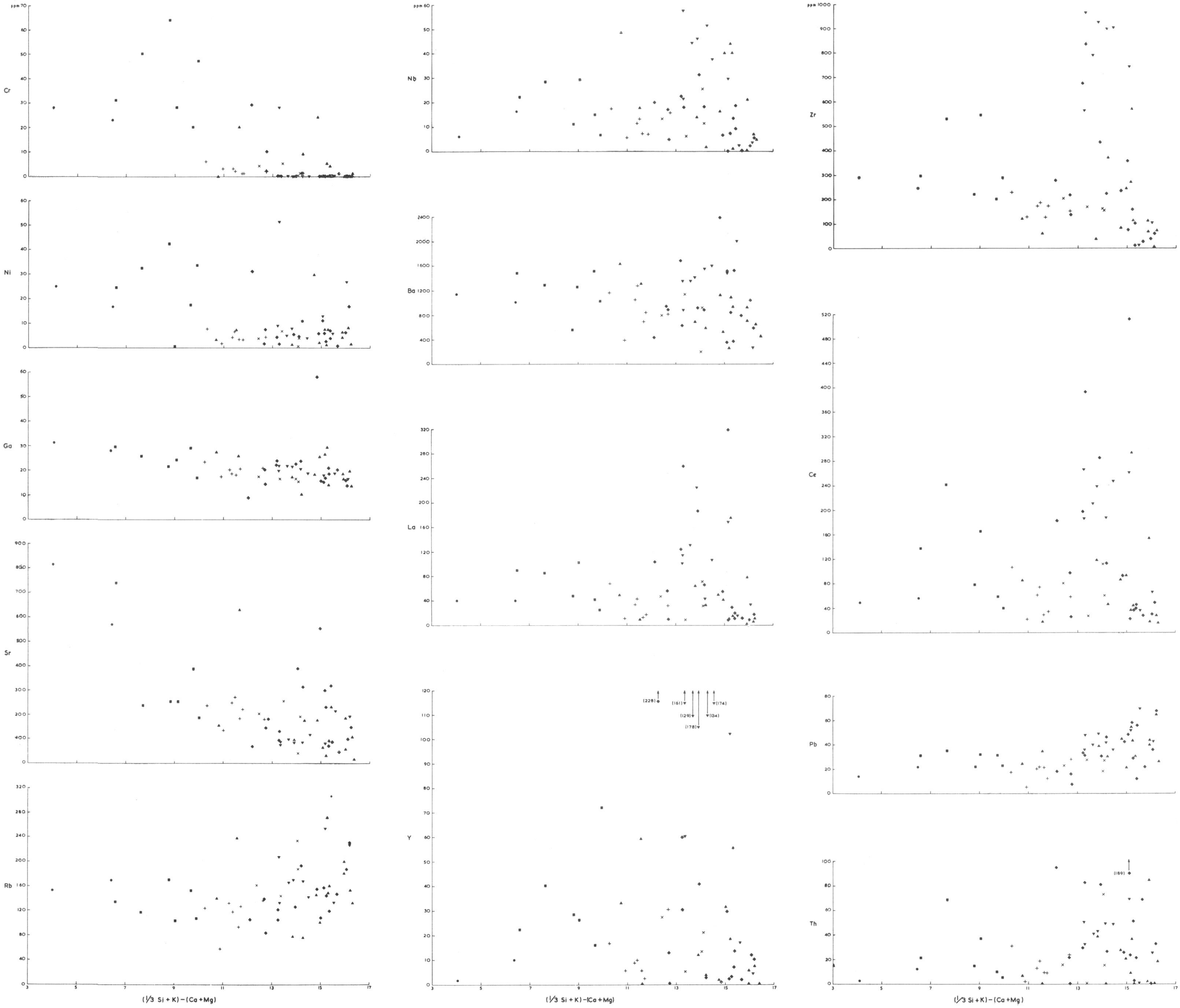

Fig. 18. Plots of trace elements (ppm) for analyses of granodiorite, augen-gneiss, granite and migmatite neosomes against the modified Larsen index (after Nockolds and Allen, 1953).
The symbols are as in Fig. 17.

face page 277

Table I. Chemical analyses of specimens of a granodiorite dyke, augen-gneisses, granites and migmatite neosomes in the Shackleton Range Metamorphic Complex

	1	2	3	4	5	6	7	8	9	10	11	12	13	14	15	16	17	18	19
SiO_2	55.26	60.14	58.63	61.83	60.12	57.80	57.72	71.00	66.71	65.40	68.71	68.78	70.79	69.79	70.54	69.32	69.42	70.08	72.46
TiO_2	1.17	0.77	1.11	1.03	0.81	0.84	0.84	0.46	0.72	0.40	0.28	0.28	0.22	0.27	0.20	0.24	0.24	0.26	0.19
Al_2O_3	16.32	15.87	15.07	15.18	16.98	15.69	15.67	14.48	14.11	16.04	15.63	15.75	15.09	15.97	15.68	15.17	15.16	15.35	14.40
Fe_2O_3	0.59	2.05	1.52	1.39	1.96	1.87	1.84	1.09	1.65	1.77	1.58	1.35	0.80	1.10	0.74	1.14	1.14	1.29	2.06
FeO	5.32	2.73	6.83	5.67	3.19	4.62	4.62	3.17	3.39	1.99	1.17	1.41	1.61	1.04	1.29	1.25	1.25	1.14	0.80
MnO	0.09	0.10	0.17	0.13	0.13	0.14	0.13	0.13	0.09	0.07	0.05	0.06	0.05	0.04	0.04	0.05	0.05	0.05	0.07
MgO	4.52	3.42	3.47	2.70	3.99	3.91	3.91	2.83	4.74	1.71	1.15	1.21	1.39	1.41	1.00	1.28	1.34	0.86	0.52
CaO	5.63	4.51	3.40	3.19	2.38	4.55	2.42	2.66	2.66	2.22	2.33	2.43	1.55	1.54	1.54	0.87	0.87	1.27	1.05
Na_2O	4.30	4.33	2.36	2.91	2.21	3.33	3.38	2.59	1.72	4.59	4.32	4.23	4.61	4.53	4.42	7.86	7.90	3.49	3.99
K_2O	2.63	2.85	3.70	4.05	5.38	3.85	3.85	2.81	3.83	3.28	3.75	3.76	3.19	3.48	4.15	1.88	1.87	5.59	4.61
P_2O_5	0.28	0.20	0.27	0.35	0.34	0.47	0.47	0.04	0.18	0.14	0.10	0.10	0.08	0.08	0.09	0.08	0.07	0.08	0.05
H_2O+	0.54	0.61	1.16	0.40	1.02	0.51	0.51	1.59	0.43	0.98	0.39	0.33	0.63	0.73	0.50	0.56	0.56	0.29	0.16
H_2O-	0.28	0.30	0.22	0.12	0.20	0.20	0.20	0.14	0.20	0.30	0.22	0.22	0.16	0.24	0.24	0.16	0.16	0.42	0.42
Total	96.93	97.88	97.91	98.95	98.71	97.78	97.69	102.75	100.43	98.89	99.68	99.91	100.17	100.22	100.43	99.86	100.03	100.17	100.78

	20	21	22	23	24	25	26	27	28	29	30	31	32	33	34	35	36	37	38	39	40
SiO_2	70.13	69.19	73.65	74.14	70.21	73.94	70.40	69.47	72.77	69.89	78.73	70.70	63.84	71.81	73.73	70.22	71.03	74.04	71.44	74.82	75.02
TiO_2	0.32	0.34	0.12	0.05	0.38	0.04	0.16	0.13	0.05	0.33	0.29	0.26	0.42	0.42	0.03	0.59	0.35	0.27	0.49	0.29	0.25
Al_2O_3	15.32	15.16	14.82	15.14	14.63	14.92	15.75	16.49	14.95	16.12	9.68	15.26	15.26	14.07	15.89	12.92	15.86	13.87	12.97	13.69	13.57
Fe_2O_3	1.03	1.45	0.39	0.11	1.21	0.16	0.67	0.41	0.58	0.15	1.71	0.58	1.56	1.58	0.00	3.16	1.19	1.34	2.59	1.97	1.65
FeO	1.55	1.75	0.43	0.33	1.98	0.22	0.61	0.44	0.66	0.45	1.98	0.90	4.32	1.39	0.32	2.71	1.37	1.09	2.78	1.41	1.32
MnO	0.06	0.07	0.02	0.02	0.05	0.01	0.02	0.01	0.03	0.02	0.05	0.03	0.19	0.06	0.01	0.10	0.05	0.04	0.16	0.05	0.05
MgO	0.99	1.05	0.16	0.20	1.55	0.28	0.39	0.19	0.14	0.28	1.51	0.63	1.22	1.08	0.35	1.23	1.04	0.87	1.06	0.46	0.54
CaO	1.50	1.95	0.71	0.73	1.17	0.53	0.78	0.74	0.51	0.94	1.33	1.26	1.04	1.42	0.73	1.34	1.02	2.06	2.07	1.76	1.16
Na_2O	3.75	3.81	4.66	4.32	3.60	2.69	2.36	4.65	4.23	4.39	1.83	2.48	3.27	2.86	2.63	3.00	3.13	3.85	2.12	3.72	2.36
K_2O	5.01	4.44	5.38	5.13	4.30	6.34	6.36	6.27	5.82	6.08	2.11	6.25	5.87	5.37	6.40	4 87	5.40	3.87	5.17	3.83	5.55
P_2O_5	0.11	0.12	0.02	0.01	0.11	0.02	0.22	0.08	0.01	0.17	0.05	0.15	0.23	0.16	0.29	0.15	0.17	0.05	0.14	0.07	0.09
H_2O+	0.16	0.13	0.08	0.21	0.83	0.14	0.08	0.07	0.19	0.17	0.39	0.22	1.11	0.32	0.07	0.21	0.52	0.20	0.13	0.19	0.29
H_2O-	0.44	0.48	0.20	0.18	0.32	0.24	0.34	0.24	0.22	0.18	0.20	0.28	0.36	0.34	0.26	0.36	0.36	0.30	0.30	0.22	0.24
Total	100.37	99.94	100.64	100.57	100.34	99.53	98.14	99.19	100.16	99.17	99.86	99.00	98.69	100 88	100.71	100 86	101.49	101.85	101.42	102.48	102.09

	41	42	43	44	45	46	47	48	49	50	51	52	53	54	55	56	57	58	59
SiO_2	73.29	72.75	74.22	72.90	74.56	72.98	72.46	65.76	72.77	73.60	53.79	73.93	82.07	71.47	73.45	62.40	73.03	74.51	76.15
TiO_2	0.34	0.36	0.33	0.43	0.19	0.03	0.24	0.65	0.02	0.12	0.15	0.05	0.13	0.42	0.07	0.72	0.28	0.16	0.05
Al_2O_3	13.14	13.05	13.24	13.69	15.49	17.16	15.09	16.55	16.57	25.71	15.13	16.39	12.25	15.19	15.78	17.50	14.41	14.66	14.41
Fe_2O_3	1.93	2.43	1.95	2.17	0.34	0.13	1.09	1.68	0.00	0.51	0.59	0.03	0.32	0.65	0.55	1.15	1.42	0.86	0.48
FeO	2.80	2.46	2.53	2.27	0.41	0.49	1.69	2.01	0.72	0.44	0.57	0.32	0.32	1.52	0.96	2.77	1.17	0.60	0.31
MnO	0.15	0.15	0.15	0.10	0.01	0.01	0.04	0.08	0.04	0.01	0.01	0.01	0.01	0.02	0.10	0.03	0.03	0.01	0.00
MgO	0.33	0.26	0.28	0.45	0.64	0.29	0.39	1.60	0.37	0.54	0.28	0.28	0.39	1.29	0.44	1.05	0.45	0.40	0.39
CaO	1.49	1.66	1.25	1.68	0.55	0.70	0.81	2.30	0.47	0.56	0.91	0.51	0.94	1.09	0.55	3.22	0.50	0.54	0.18
Na_2O	3.32	3.19	2.63	3.17	2.76	3.52	3.60	4.67	3.26	2.77	6.15	3.27	3.06	1.93	4.09	1.72	3.90	4.93	3.91
K_2O	4.46	5.11	4.84	4.53	6.34	5.84	5.73	3.79	6.23	6.32	3.85	6.26	2.88	6.33	5.51	5.83	5.43	4.85	5.79
P_2O_5	0.10	0.10	0.11	0.13	0.09	0.05	0.11	0.18	0.12	0.06	0.08	0.06	0.03	0.05	0.07	0.09	0.05	0.03	0.02
H_2O+	0.27	0.16	0.33	0.57	0.29	0.45	0.37	0.45	0.41	0.40	0.13	0.37	0.14	0.47	0.29	0.63	0.16	0.11	0.16
H_2O-	0.20	0.20	0.24	0.18	0.12	0.20	0.20	0.18	0.14	0.16	0.14	0.12	0.34	0.26	0.22	0 22	0.22	0.20	0.20
Total	101.82	101.88	102.10	102.27	101.79	101.85	101.82	99.90	101.12	101.20	101.78	101.60	102.88	100.69	102.08	97.33	101.05	101.86	102.05

ANALYSES RECALCULATED TO 100% ANHYDROUS

	1	2	3	4	5	6	7	8	9	10	11	12	13	14	15	16	17	18	19
SiO_2	57.50	62.02	60.74	62.82	61.67	59.54	59.52	70.28	66.84	67.00	69.36	69.22	71.23	70.32	70.76	69.92	69.90	70.46	72.32
TiO_2	1.22	0.79	1.15	1.05	0.83	0.87	0.87	0.46	0.72	0.41	0.28	0.28	0.22	0.27	0.20	0.24	0.24	0.26	0.19
Al_2O_3	16.98	16.37	15.61	15.42	17.42	16.16	16.16	14.33	14.14	16.43	15.78	15.85	15.18	16.09	15.73	15.30	15.27	15.43	14.37
Fe_2O_3	0.61	2.11	1.57	1.41	2.01	1.93	1.90	1.08	1.65	1.81	1.59	1.36	0.80	1.11	0.74	1.15	1.15	1.30	2.06
FeO	5.54	2.02	7.08	5.76	3.27	4.76	4.76	3.14	3.40	2.04	1.18	1.42	1.62	1.05	1.29	1.26	1.26	1.15	0.80
MnO	0.09	0.10	0.18	0.13	0.13	0.14	0.13	0.13	0.09	0.07	0.05	0.06	0.05	0.04	0.04	0.05	0.05	0.05	0.07
MgO	4.70	3.53	3.59	2.74	4.09	4.03	4.03	2.80	4.75	1.75	1.16	1.22	1.40	1.42	1.00	1.29	1.35	0.86	0.52
CaO	5.86	4.65	3.52	3.24	2.44	4.69	4.69	2.40	2.67	2.27	2.35	2.45	1.56	1.55	1.54	0.88	0.88	1.28	1.05
Na_2O	4.47	4.47	2.44	2.96	2.27	3.43	3.49	2.56	1.72	4.70	4.36	4.26	4.64	4.56	4.43	7.93	7.95	3.51	3.98
K_2O	2.74	2.94	3.83	4.11	5.52	3.97	3.97	2.78	3.84	3.36	3.79	3.78	3.21	3.51	4.16	1.90	1.88	5.62	4.60
P_2O_5	0.29	0 21	0.28	0.36	0.35	0.48	0.48	0.04	0.18	0.14	0.10	0.10	0.08	0.08	0.09	0.08	0.07	0.08	0.05

	20	21	22	23	24	25	26	27	28	29	30	31	32	33	34	35	36	37	38	39	40
SiO_2	70.29	69.66	73.39	74.01	70.78	74.57	72.04	70.26	72.95	70.72	79.31	71.78	65.67	71.65	73.45	70.02	70.60	73.05	70.74	73.30	73.87
TiO_2	0.32	0.34	0.12	0.05	0.38	0.04	0.16	0.13	0.05	0.33	0.29	0.26	0.43	0.42	0.03	0.59	0.35	0.27	0.49	0.28	0.25
Al_2O_3	15.36	15.26	14.77	15.11	14.75	15.05	16.12	16.68	14.99	16.31	9.75	15.49	15.70	14.04	15.83	12.88	15.76	13.69	12.84	13.41	13.36
Fe_2O_3	1.03	1.46	0.39	0.11	1.22	0.16	0.69	0.41	0.58	0.15	1.72	0.59	1.60	1.58	0.00	3.15	1.18	1.32	2.56	1.93	1.62
FeO	1.55	1.76	0.43	0.33	2.00	0.22	0.62	0.44	0.66	0.46	1.99	0.91	4.44	1.39	0.32	2.70	1.36	1.08	2.75	1.38	1.30
MnO	0.06	0.07	0.02	0.02	0.05	0.01	0.02	0.01	0.03	0.02	0.05	0.03	0.20	0.06	0.01	0.10	0.05	0.04	0.16	0.05	0.05
MgO	0.99	1.06	0.16	0.20	1.56	0.28	0.40	0.19	0.14	0.28	1.52	0.64	1.25	1.08	0.35	1.23	1.03	0.86	1.05	0.45	0.53
CaO	1.50	1.96	0.71	0.73	1.18	0.53	0.80	0.75	0.51	0.95	1.34	1.28	1.07	1.42	0.73	1.34	1.01	2.03	2.05	1.72	1.14
Na_2O	3.76	3.84	4.64	4.31	3.63	2.71	2.42	4.70	4.24	4.44	1.84	2.52	3.36	2.85	2.62	2.99	3.11	3.80	2.10	3.64	2.32
K_2O	5.02	4.47	5.36	5.12	4.34	6.39	6.51	6.34	5.83	6.15	2.13	6.35	6.04	5.36	6.38	4.86	5.37	3.82	5.12	3.75	5.46
P_2O_5	0.11	0.12	0 02	0.01	0.11	0.02	0.23	0.08	0.01	0.17	0.05	0.15	0.24	0.16	0.29	0.15	0.17	0.05	0.14	0.07	0.09

	41	42	43	44	45	46	47	48	49	50	51	52	53	54	55	56	57	58	59
SiO_2	72.31	71.66	73.10	71.81	73.55	72.11	71.57	66.24	72.36	73.13	72.69	73.12	80.15	71.50	72.31	64.68	72.54	73.37	74.88
TiO_2	0.34	0.35	0.33	0.42	0.19	0.03	0.24	0.65	0.02	0.12	0.15	0.05	0.13	0.42	0.07	0.75	0.28	0.16	0.05
Al_2O_3	12.96	12.85	13.04	13.49	15.28	16.96	14.90	16.67	16.48	15.61	14.90	16.21	11.96	15.20	15.54	18.14	14.31	14.44	14.17
Fe_2O_3	1.90	2.39	1.92	2.14	0.34	0.13	1.08	1.69	0.00	0.51	0.58	0.03	0.31	0.65	0.54	1.19	1.41	0.85	0.47
FeO	2.76	2.42	2.49	2.24	0.40	0.48	1.67	2.02	0.72	0.44	0.56	0.32	0.31	1.52	0.95	2.87	1.16	0.59	0.30
MnO	0.15	0.15	0.15	0.10	0.01	0.01	0 04	0.08	0.04	0.01	0.01	0.01	0.01	0.02	0.10	0.03	0.03	0.01	0.00
MgO	0.33	0.26	0.28	0.44	0.63	0.29	0.39	1.61	0.37	0.54	0.28	0.28	0.38	1.29	0.43	1.09	0.45	0.39	0.38
CaO	1.47	1.64	1.23	1.65	0.54	0.69	0.80	2.32	0.47	0.56	0.90	0.50	0.92	1.09	0.54	3.34	0.50	0.53	0.18
Na_2O	3.28	3.14	2.59	3.12	2.72	3.48	3.56	4.70	3.24	2.75	6.06	3.23	2.99	1.93	4.03	1.78	3.87	4.85	3.85
K_2O	4.40	5.03	4.77	4.46	6.25	5.77	5.66	3.82	6.19	6.28	3.79	6.19	2.81	6.33	5.42	6.04	5.39	4.78	5.69
P_2O_5	0.10	0.10	0.11	0.13	0.09	0.05	0.11	0.18	0.12	0.06	0.08	0.06	0.03	0.05	0.07	0.09	0.05	0.03	0.02

C.I.P.W. NORMS

	1	2	3	4	5	6	7	8	9	10	11	12	13	14	15	16	17	18	19
Q	0.49	10.22	14.90	16.00	15.29	7.50	7.18	33.41	27.96	18.74	22.59	22.51	25.71	24.69	23.65	13.16	12.98	24.25	28.58
c			1.57	0.93	3.93			2.78	2.66	1.14	0.34	0.43	1.35	2.06	1.25			1.34	1.03
zc	0.06	0.05	0.11	0.11	0.04	0.06	0.06	0.06	0.04	0.05	0.04	0.03	0.03	0.03	0.03	0.03	0.03	0.03	0.03
or	16.19	17.40	22.65	24.31	32.61	23.44	23.46	16.46	22.71	19.88	22.38	22.38	18.99	20.74	24.62	11.20	11.12	33.24	27.25
ab	37.79	37.73	20.65	24.97	19.15	28.97	29.43	21.68	14.57	39.74	36.85	35.99	39.22	38.59	37.48	67.05	67.27	29.66	33.68
an	18.11	15.88	15.96	14.07	10.26	16.94	16.67	11.77	12.20	10.65	11.35	11.76	7.41	7.41	7.29	0.57	0.39	6.05	4.91
di	7.77	4.95				2.99	3.22									2.71	2.90		
hy	15.70	8.71	19.04	14.73	13.40	14.53	14.44	11.32	15.66	6.06	3.37	4.16	5.52	4.17	4.00	2.97	3.03	2.85	1.29
mt	0.89	3.06	2.28	2.04	2.91	2.79	2.75	1.56	2.40	2.63	2.31	1.97	1.17	1.61	1.08	1.67	1.66	1.88	2.25
il	2.31	1.51	2.18	1.98	1.58	1.64	1.64	0.86	1.37	0.78	0.54	0.53	0.42	0.52	0.38	0.46	0.46	0.50	0.36
ap	0.69	0.49	0.66	0.84	0.82	1.14	1.14	0.09	0 43	0.34	0.24	0.24	0.19	0.19	0.21	0.19	0.17	0.19	0.12
Plagioclase composition	An_{32}	An_{30}	An_{44}	An_{36}	An_{35}	An_{37}	An_{36}	An_{35}	An_{46}	An_{21}	An_{24}	An_{25}	An_{16}	An_{16}	An_{16}	An_{1}	An_{1}	An_{17}	An_{13}
Q	1	16	26	25	23	13	12	47	43	24	28	28	31	29	28	15	14	28	32
or	30	26	35	38	28	48	49	30	22	25	27	28	23	25	29	12	12	38	30
ab	69	58	39	37	49	39	39	23	35	51	45	44	46	46	43	73	74	34	38
or	23	25	38	38	53	34	34	33	46	28	32	32	29	31	35	14	14	48	41
ab	52	53	35	40	31	42	42	43	29	57	52	51	60	58	54	85	85	43	51
an	25	22	27	22	16	24	24	24	25	15	16	17	11	11	11	1	1	9	8

	20	21	22	23	24	25	26	27	28	29	30	31	32	33	34	35	36	37	38	39	40
Q	23.91	23.91	23.90	27.17	27.40	32.57	31.12	16.63	24.25	19.03	54.50	28.83	16.39	18.83	2.16	28.77	28.05	30.70	31.97	33.12	35.81
c	1.14	0.74	0.02	1.11	2.11	2.66	4.13	0.75	0.72	0.87	2.06	2.26	2.17	1.23	3.91	0.49	3.28		0.33	0.30	1.62
zc	0.03	0.04	0.03	0.02	0.04		0.02			0.07	0.06	0.05	0.17	0.09		0.14	0.04	0.03	0.19	0.11	0.15
or	29.69	26.44	31.70	30.30	25.64	37.84	38.53	37.48	34.51	36.34	12.59	37.48	35.65	31.66	37.71	28.68	31.74	22.55	30.25	22.19	32.31
ab	31.77	32.42	39.26	36.47	30.68	22.94	20.42	39.75	35.86	37.53	15.59	21.26	28.41	24.11	22.15	25.26	26.29	32.12	17.72	30.80	19.62
an	7.05	9.17	3.55	3.69	5.37	2.69	2.60	3.59	2.63	4.00	6.40	6.01	3.93	6.29	1.90	6.02	4.20	9.01	9.55	8.31	5.41
di																		0.79			
hy	4.05	4.22	0.70	0.97	6.00	0.93	1.34	0.75	1.06	0.90	5.63	2.40	9.59	3.34	1.42	4.62	3.61	2.28	5.03	1.68	2.05
mt	1.50	2.11	0.56	0.16	1.77	0.23	0.99	0.60	0.84	0.22	2.50	0.85	2.32	2.28		4.56	1.71	1.92	3.71	2.79	2.35
il	0.61	0.65	0.23	0.09	0.73	0.08	0.31	0.25	0.10	0.63	0.55	0.50	0.82	0.79	0.06	1.12	0.66	0.51	0.92	0.54	0.47
ap	0.26	0.29	0.05	0.02	0.26	0.05	0.53	0.19	0.02	0.41	0.12	0.36	0.56	0.38	0.68	0.35	0.40	0.12	0.33	0.16	0.21
Plagioclase composition	An_{18}	An_{22}	An_{8}	An_{9}	An_{15}	An_{10}	An_{11}	An_{8}	An_{7}	An_{10}	An_{29}	An_{22}	An_{12}	An_{21}	An_{8}	An_{19}	An_{14}	An_{22}	An_{35}	An_{21}	An_{22}
Q	28	29	25	29	33	35	34	18	26	21	66	33	21	35	35	35	33	36	40	38	41
or	35	32	33	32	37	41	43	40	36	39	15	43	44	28	24	30	30	38	22	36	22
ab	37	39	42	39	30	24	23	42	38	40	19	24	35	37	41	35	37	26	38	26	37
or	43	39	42	43	41	60	63	46	47	47	36	58	52	51	61	48	51	35	53	36	56
ab	47	48	53	52	50	36	33	49	49	48	45	33	42	39	36	42	42	51	31	50	34
an	10	13	5	5	9	4	4	5	4	5	19	9	6	10	3	10	7	14	16	14	10

	41	42	43	44	45	46	47	48	49	50	51	52	53	54	55	56	57	58	59
Q	31.31	29.61	35.49	31.62	31.65	27.43	26.28	16.56	27.80	31.05	21.00	28.99	49.35	31.00	25.73	20.97	27.31	25.05	29.70
c	0.25		1.50	0.69	3.14	3.66	1.70	0.87	3.77	3.35		3.37	2.34	3.19	2.11	2.62	1.22	0.34	1.35
zc	0.18	0.18	0.18	0.16	0.02		0.05	0.02		0.02			0.07	0.02	0 02		0.11	0.05	
or	26.01	29.74	28.16	26.37	37.00	34.11	33.51	22.58	36.65	37.15	22.40	36.62	16.61	37.44	32.08	35.74	31.88	28.24	33.68
ab	27.66	26.53	21.87	26.37	23.01	29.40	30.06	39.76	27.41	23.27	51.24	27.36	25.26	16.32	34.04	15.07	32.73	41.05	32.52
an	6.95	6.07	5.75	7.67	2.38	3.58	3.32	10.69	1.79	2.52	2.27	2.21	4.53	5.37	2.50	16.42	2.39	2.55	0.89
di		1.48									1.48								
hy	4.02	2.03	3.41	2.92	1.74	1.46	2.81	5.40	2.27	1.54	0.29	1.18	1.07	4.81	2.43	5.82	1.68	1.12	1.04
mt	2.76	3.46	2.78	3.09	0.49	0.19	1.56	2.45		0.73	0.84	0.04	0.45	0.94	0.78	1.73	2.04	1.23	0.68
il	0.64	0.67	0.62	0.80	0.36	0.06	0.45	1.24	0.04	0.23	0.28	0.09	0.24	0.80	0.13	1.42	0.53	0.30	0.09
ap	0.23	0.23	0.26	0.30	0.21	0.12	0.26	0.43	0.28	0.14	0.19	0.14	0.07	0.12	0.16	0.22	0.12	0.07	0.05
Plagioclase composition	An_{20}	An_{19}	An_{21}	An_{23}	An_{9}	An_{11}	An_{10}	An_{21}	An_{6}	An_{10}	An_{4}	An_{7}	An_{15}	An_{25}	An_{7}	An_{52}	An_{7}	An_{6}	An_{3}
Q	37	34	41	38	35	30	29	21	30	34	22	31	54	37	28	29	30	27	31
or	33	31	26	31	25	32	34	50	30	25	54	29	28	19	37	21	35	43	34
ab	30	35	33	31	40	38	37	29	40	41	24	40	18	44	35	50	25	30	35
or	43	48	51	44	59	51	50	31	56	59	29	56	36	63	47	53	48	39	50
ab	46	42	39	44	37	44	45	54	41	37	68	41	54	28	50	22	49	57	49
an	11	10	10	12	4	5	5	15	3	4	3	3	10	9	3	25	3	4	1

ELEMENT WEIGHT PERCENTAGES, ANHYDROUS

	1	2	3	4	5	6	7	8	9	10	11	12	13	14	15	16	17	18	19
Si^{4+}	26.88	28.99	28.39	29.37	28.83	27.84	27.82	32.86	31.25	31.32	32.42	32.36	33.30	32.87	33.08	32.69	32.68	32.94	33.81
Ti^{4+}	0.73	0.48	0.69	0.63	0.50	0.52	0.52	0.27	0.43	0.25	0.17	0.17	0.13	0.16	0.12	0.15	0.14	0.16	0.11
Al^{3+}	8.99	8.66	8.26	8.16	9.22	8.55	8.55	7.59	7.48	8.70	8.35	8.39	8.04	8.52	8.32	8.10	8.08	8.17	7.61
Fe^{3+}	0.43	1.48	1.10	0.99	1.41	1.35	1.33	0.75	1.16	1.27	1.12	0.95	0.56	0.78	0.52	0.80	0.80	0.91	1.44
Fe^{2+}	4.30	2.19	5.50	4.48	2.54	3.70	3.70	2.44	2.64	1.58	0.92	1.10	1.26	0.81	1.01	0.98	0.98	0.89	0.62
Mn^{2+}	0.07	0.08	0.14	0.10	0.10	0.11	0.10	0.10	0.07	0.06	0.04	0.05	0.04	0.03	0.03	0.04	0.04	0.04	0.05
Mg^{2+}	2.84	2.13	2.17	1.65	2.47	2.43	2.43	1.69	2.86	1.06	0.70	0.73	0.84	0.86	0.61	0.78	0.81	0.52	0.31
Ca^{2+}	4.19	3.32	2.52	2.32	1.74	3.35	3.35	1.71	1.90	1.63	1.68	1.75	1.11	1.11	1.10	0.63	0.63	0.91	0.75
Na^{+}	3.32	3.31	1.81	2.19	1.68	2.55	2.59	1.90	1.28	3.49	3.24	3.16	3.44	3.39	3.29	5.88	5.90	2.60	2.95
K^{+}	2.27	2.44	3.18	3.42	4.58	3.29	3.30	2.30	3.19	2.79	3.14	3.14	2.66	2.91	3.46	1.57	1.56	4.67	3.82
P^{5+}	0.13	0.09	0.12	0.16	0.15	0.21	0.21	0.02	0.08	0.06	0.04	0.04	0.04	0.04	0.04	0.04	0.03	0.04	0.02
O^{2-}	45.86	46.83	46.11	46.54	46.77	46.10	46.09	48.36	47.66	47.80	48.18	48.15	48.57	48.53	48.43	48.35	48.34	48.16	48.50

	20	21	22	23	24	25	26	27	28	29	30	31	32	33	34	35	36	37	38	39	40
Si^{4+}	32.86	32.56	34.31	34.60	33.09	34.86	33.68	32.85	34.11	33.06	37.08	33.56	30.70	33.50	34.34	32.73	33.01	34.15	33.07	34.27	34.53
Ti^{4+}	0.19	0.21	0.07	0.03	0.23	0.02	0.10	0.08	0.03	0.20	0.18	0.16	0.26	0.25	0.02	0.35	0.21	0.16	0.29	0.17	0.15
Al^{3+}	8.13	8.08	7.81	8.00	7.81	7.96	8.53	8.83	7.93	8.63	5.16	8.20	8.31	7.43	8.38	6.82	8.34	7.24	6.80	7.10	7.07
Fe^{3+}	0.72	1.02	0.27	0.08	0.85	0.11	0.48	0.29	0.41	0.11	1.20	0.40	1.12	1.10	0.00	2.20	0.83	0.92	1.79	1.35	1.14
Fe^{2+}	1.21	1.37	0.33	0.26	1.55	0.17	0.49	0.35	0.51	0.35	1.55	0.71	3.45	1.08	0.25	2.10	1.06	0.84	2.14	1.07	1.01
Mn^{2+}	0.05	0.05	0.02	0.02	0.04	0.01	0.02	0.01	0.02	0.02	0.04	0.02	0.15	0.05	0.01	0.08	0.04	0.03	0.12	0.04	0.04
Mg^{2+}	0.60	0.64	0.10	0.12	0.94	0.17	0.24	0.12	0.08	0.17	0.92	0.39	0.76	0.65	0.21	0.74	0.62	0.52	0.63	0.27	0.32
Ca^{2+}	1.07	1.40	0.51	0.52	0.84	0.38	0.57	0.53	0.37	0.68	0.96	0.91	0.76	1.01	0.52	0.95	0.72	1.45	1.46	1.23	0.82
Na^{+}	2.79	2.85	3.44	3.20	2.69	2.01	1.79	3.49	3.15	3.30	1.37	1.87	2.50	2.12	1.94	2.22	2.31	2.82	1.56	2.70	1.72
K^{+}	4.17	3.71	4.45	4.25	3.60	5.31	5.40	5.26	4.84	5.11	1.76	5.27	5.01	4.45	5.29	4.03	4.46	3.17	4.25	3.11	4.54
P^{5+}	0.05	0.05	0.01	0.00	0.05	0.01	0.10	0.04	0.00	0.08	0.02	0.07	0.10	0.07	0.13	0.07	0.07	0.02	0.06	0.03	0.04
O^{2-}	48.17	48.06	48.68	48.93	48.30	48.97	48.61	48.17	48.55	48.30	49.76	48.44	46.88	48.30	48.92	47.71	48.33	48.67	47.82	48.65	48.63

	41	42	43	44	45	46	47	48	49	50	51	52	53	54	55	56	57	58	59
Si^{4+}	33.81	33.50	34.17	33.57	34.38	33.71	33.46	30.97	33.83	34.19	33.98	34.18	37.47	33.43	33.81	30.24	33.91	34.30	35.01
Ti^{4+}	0.20	0.21	0.19	0.25	0.11	0.02	0.14	0.39	0.01	0.07	0.09	0.03	0.08	0.25	0.04	0.45	0.17	0.09	0.03
Al^{3+}	6.86	6.80	6.90	7.14	8.09	8.97	7.89	8.82	8.72	8.26	7.89	8.58	6.33	8.04	8.22	9.60	7.58	7.64	7.50
Fe^{3+}	1.33	1.67	1.34	1.49	0.23	0.09	0.75	1.18	0.00	0.35	0.41	0.02	0.22	0.45	0.38	0.83	0.99	0.59	0.33
Fe^{2+}	2.15	1.88	1.94	1.74	0.31	0.38	1.30	1.57	0.56	0.34	0.44	0.25	0.24	1.18	0.73	2.23	0.90	0.46	0.24
Mn^{2+}	0.11	0.11	0.11	0.08	0.01	0.01	0.03	0.06	0.03	0.01	0.01	0.01	0.01	0.02	0.08	0.02	0.02	0.01	0.00
Mg^{2+}	0.20	0.15	0.17	0.27	0.38	0.17	0.23	0.97	0.22	0.32	0.17	0.17	0.23	0.78	0.26	0.66	0.27	0.24	0.23
Ca^{2+}	1.05	1.17	0.88	1.18	0.39	0.49	0.57	1.66	0.33	0.40	0.64	0.36	0.66	0.78	0.39	2.39	0.35	0.38	0.13
Na^{+}	2.43	2.33	1.92	2.32	2.02	2.58	2.64	3.49	2.40	2.04	4.49	2.40	2.22	1.43	2.99	1.32	2.87	3.60	2.85
K^{+}	3.65	4.18	3.96	3.70	5.19	4.79	4.70	3.17	5.14	5.21	3.15	5.14	2.33	5.26	4.50	5.02	4.48	3.96	4.73
P^{5+}	0.04	0.04	0.05	0.06	0.04	0.02	0.05	0.08	0.05	0.03	0.03	0.03	0.01	0.02	0.03	0.04	0.02	0.01	0.01
O^{2-}	48.16	47.94	48.36	48.20	48.84	48.76	48.25	47.63	48.70	48.77	48.70	48.84	50.21	48.36	48.57	47.21	48.43	48.71	48.95

TRACE ELEMENTS (ppm)

	1	2	3	4	5	6	7	8	9	10	11	12	13	14	15	16	17	18	19
Cr	28	23	50	28	20	31	31	47	64	6	2	3	1	1	2	4	1	1	*
Ni	25	17	32	*	17	20	27	33	42	8	7	5	4	4	5	2	2	4	1
Ga	32	29	26	24	29	29	28	17	22	24	19	20	19	21	21	17	18	16	17
Rb	152	170	97	102	153	131	132	106	168	125	122	134	97	129	132	60	59	190	238
Sr	818	571	239	255	390	742	741	192	160	243	278	255	189	224	181	143	142	194	45
Y	1	9	40	26	16	22	22	72	28	16	9	8	5	2	30	4	5	21	13
Zr	288	245	531	545	200	296	308	290	222	228	185	171	125	172	152	125	125	154	162
Nb	7	17	28	29	15	23	20	7	11	18	14	12	8	8	17	5	7	12	26
Ba	1 167	1 029	1 254	1 273	1 533	1 514	1 498	486	585	1 158	1 276	1 062	701	835	816	403	391	927	207
La	41	42	87	104	43	102	101	28	52	67	43	34	14	17	32	14	12	33	72
Ce	53	56	239	165	56	134	138	38	76	109	76	61	31	36	59	24	28	61	112
Pb	15	22	34	31	30	27	30	22	21	18	21	20	21	12	27	7	4	26	18
Th	3	13	68	36	9	21	20	5	14	32	20	13	5	5	24	3	*	16	75

	20	21	22	23	24	25	26	27	28	29	30	31	32	33	34	35	36	37	38	39	40
Cr	5	4	*	*	2	*	*	*	1	*	29	*	*	*	*	*	1	10	28	*	*
Ni	7	4	2	6	1	17	4	7	1	11	31	6	2	5	6	4	4	7	51	9	13
Ga	17	18	17	16	20	14	21	19	20	16	9	58	24	22	16	22	23	15	22	20	18
Rb	146	163	146	160	137	232	303	123	150	110	103	158	108	123	186	120	182	82	206	131	253
Sr	258	206	74	233	150	147	92	318	51	301	74	555	133	391	106	101	321	183	85	90	90
Y	5	27	3	2	13	10	13	7	2	29	228	*	30	41	12	60	3	*	161	60	102
Zr	164	201	161	75	219	57	101	9	24	358	281	235	831	437	36	678	223	138	959	566	745
Nb	7	14	14	8	17	6	19	10	*	*	20	7	19	31	2	22	18	5	57	21	29
Ba	1 143	798	851	359	967	602	391	1 516	808	1 522	444	2 378	651	946	721	1 711	902	924	1 383	921	1 549
La	10	48	29	10	60	18	20	13	13	318	105	57	258	189	10	126	68	13	105	116	170
Ce	27	81	38	24	96	47	44	41	28	509	184	94	393	285	27	194	110	23	264	183	258
Pb	27	22	28	57	15	66	55	12	21	47	18	41	33	29	34	32	43	7	46	34	50
Th	*	16	52	24	22	34	22	3	70	189	95	25	84	80	*	29	26	*	49	32	69

	41	42	43	44	45	46	47	48	49	50	51	52	53	54	55	56	57	58	59
Cr	*	*	*	*	*	*	5	*	*	*	*	*	9	24	4	20	*	*	1
Ni	8	11	4	5	27	6	7	3	4	6	1	8	11	30	7	7	1	2	2
Ga	21	21	19	24	17	19	27	28	17	19	17	20	12	18	14	26	29	26	14
Rb	169	166	140	164	228	132	271	138	201	181	77	151	77	144	159	235	147	101	131
Sr	88	90	115	106	195	222	36	162	188	65	98	111	173	168	236	625	95	71	27
Y	178	134	174	129	5	17	19	33	*	6	12	8	4	2	7	*	56	32	1
Zr	925	898	910	786	104	17	272	120	67	109	29	*	377	86	108	59	568	245	71
Nb	46	51	37	44	4	2	44	48	*	21	14	7	2	16	1	18	40	40	5
Ba	1 426	1 559	1 624	1 382	1 056	2 040	298	1 649	967	746	735	296	618	1 168	983	1 348	1 099	553	686
La	224	46	108	132	35	17	12	54	3	82	67	9	35	51	17	16	178	44	14
Ce	236	182	245	208	64	32	35	84	16	152	117	23	49	84	39	16	291	92	22
Pb	46	40	34	38	41	68	54	24	39	43	38	63	25	43	30	34	42	20	25
Th	41	39	48	41	25	*	9	6	2	87	41	*	*	28	*	*	37	21	18

INDICES, TRIANGULAR COORDINATES AND RATIOS

	1	2	3	4	5	6	7	8	9	10	11	12	13	14	15	16	17	18	19
Index†	4.03	6.44	7.67	9.07	9.71	6.58	6.57	9.94	8.80	10.28	11.45	11.36	11.72	11.80	12.72	10.95	10.92	14.12	14.04
Fe	36.0	31.8	48.0	42.9	31.1	37.9	37.7	35.1	34.1	28.0	22.3	22.6	20.8	18.2	17.2	17.8	17.7	18.8	22.5
Mg	21.6	18.4	15.8	13.0	19.5	18.2	18.2	18.6	25.7	10.4	7.7	8.1	9.6	9.8	6.8	7.8	8.1	5.4	3.4
Alk	42.5	49.8	36.3	44.1	49.4	43.8	44.1	46.3	40.1	61.6	70.0	69.3	69.6	72.0	76.0	74.4	74.2	75.8	74.1
Ca	42.8	36.6	33.5	29.2	21.8	36.5	36.3	28.9	29.9	20.6	20.9	21.7	15.4	15.0	14.1	7.8	7.7	11.2	10.0
Na	33.9	36.5	24.1	27.7	21.0	27.7	28.0	32.1	20.1	44.1	40.1	39.2	47.7	45.7	41.9	72.8	72.9	31.8	39.3
K	23.2	26.9	42.4	43.1	57.2	35.8	35.7	39.0	50.0	35.3	39.0	39.0	36.9	39.3	44.0	19.5	19.3	57.0	50.8
K/Rb	143.6	139.2	316.6	329.6	291.9	244.0	242.1	220.1	189.2	217.8	255.2	232.9	273.0	223.9	261.0	260.1	263.1	244.2	160.8
K/Ba	18.71	22.99	24.49	26.41	29.13	21.11	21.33	48.00	54.35	23.51	24.40	29.39	37.77	34.60	42.22	38.72	39.70	50.06	184.87
Ti/Zr	25.3	19.6	13.0	11.6	25.0	17.6	16.9	9.3	19.4	11.0	9.2	9.9	10.4	9.3	7.9	12.0	11.2	10.4	6.8
Ba/Sr	1.43	1.80	5.25	4.99	3.93	2.04	2.02	2.53	3.66	4.77	4.59	4.17	3.71	3.73	4.51	2.82	2.75	4.78	4.60
Rb/Sr	0.19	0.30	0.41	0.40	0.39	0.18	0.18	0.55	1.05	0.51	0.44	0.53	0.51	0.58	0.73	0.42	0.42	0.98	5.29
Ce/La	1.29	1.33	2.75	1.59	1.30	1.31	1.37	1.36	1.46	1.63	1.77	1.79	2.21	2.12	1.97	1.71	2.33	1.85	1.56
Ba/Rb	7.68	6.05	12.93	12.48	10.02	11.56	11.35	4.58	3.48	9.26	10.46	7.93	7.23	6.47	6.18	6.72	6.63	4.88	0.87

	20	21	22	23	24	25	26	27	28	29	30	31	32	33	34	35	36	37	38	39	40
Index†	13.40	12.42	15.32	15.15	12.72	16.22	15.44	15.37	15.71	15.08	12.14	14.91	13.33	13.96	16.05	13.27	14.18	12.74	13.29	13.29	15.13
Fe	20.3	24.9	7.0	4.2	24.9	3.7	11.5	6.7	10.2	5.1	40.5	13.0	35.6	23.2	3.2	38.1	20.3	21.3	37.9	28.5	24.6
Mg	6.3	6.7	1.1	1.5	9.8	2.2	2.9	1.2	0.9	1.9	13.5	4.5	5.9	6.9	2.7	6.6	6.7	6.3	6.1	3.2	3.7
Alk	73.3	68.4	91.8	94.3	65.3	94.1	85.6	92.1	88.8	93.0	46.0	82.6	58.5	69.9	94.0	55.3	72.9	72.4	56.0	68.3	71.7
Ca	13.4	17.6	6.0	6.5	11.8	5.0	7.3	5.8	4.4	7.5	23.4	11.4	9.2	13.4	6.7	13.3	9.7	19.5	20.1	17.5	11.5
Na	34.7	35.8	41.0	40.1	37.7	26.1	23.1	37.6	37.7	36.3	33.4	23.2	30.2	27.9	25.1	30.8	30.8	37.9	21.4	38.3	24.4
K	51.9	46.6	53.0	53.3	50.4	68.9	69.6	56.7	58.0	56.2	43.1	65.4	60.6	58.7	68.2	55.9	59.5	42.6	58.4	44.2	64.1
K/Rb	284.8	226.1	305.9	266.2	260.5	226.8	174.2	423.1	322.1	458.8	170.0	328.4	451.2	362.4	285.6	336.9	246.3	391.8	208.3	242.7	182.1
K/Ba	36.38	46.19	52.48	118.62	39.61	87.42	35.02	34.33	59.79	33.16	39.45	21.82	74.85	47.12	73.68	23.63	49.70	34.77	31.03	34.52	29.74
Ti/Zr	11.6	10.4	4.3	4.0	10.5	3.5	9.9	88.9	12.5	5.6	6.4	6.8	3.1	5.7	5.6	5.2	9.4	11.6	3.0	3.0	2.0
Ba/Sr	4.43	3.87	1.50	1.54	6.45	4.10	4.25	4.77	5.84	5.06	6.00	4.29	4.90	2.42	6.80	16.94	2.81	5.05	16.27	10.23	17.21
Rb/Sr	0.57	0.79	1.97	0.69	0.91	1.58	3.29	0.39	2.94	0.37	1.39	0.29	0.81	0.32	1.76	1.19	0.57	0.45	2.42	1.46	2.81
Ce/La	2.70	1.69	1.31	2 40	1.60	2.61	2.20	3.15	2.15	1.60	1.75	1.65	1.52	1.51	2.70	1.54	1.62	1.77	2.51	1.58	1.52
Ba/Rb	7.83	4.90	5.83	2.24	7.06	2.59	1.29	12.33	5.39	13.84	4.31	15.05	6.03	7.69	3.88	14.26	4.96	11.27	6.71	7.03	6.12

	41	42	43	44	45	46	47	48	49	50	51	52	53	54	55	56	57	58	59
Index†	13.84	14.22	14.50	13.63	16.09	15.53	15.22	10.77	15.94	15.97	13.86	16.17	14.25	14.82	15.34	11.61	15.24	14.99	16.29
Fe	35.7	34.8	35.2	34.0	6.7	5.8	21.3	26.5	6.7	8.4	9.7	3.3	8.8	18.0	12.6	30.5	19.9	11.9	6.8
Mg	2.0	1.5	1.8	2.8	4.7	2.2	2.4	9.4	2.7	3.9	1.9	2.1	4.4	8.6	2.9	6.5	2.8	2.7	2.8
Alk	62.3	63.7	63.0	63.2	88.6	92.0	76.3	64.1	90.7	87.7	88.3	94.6	86.8	73.5	84.5	63.0	77.3	85.8	90.5
Ca	14.7	15.2	13.0	16.4	5.1	6.3	7.2	19.9	4.2	5.2	7.7	4.6	12.6	10.4	4.9	27.3	4.6	4.8	1.6
Na	34.1	30.4	28.4	32.2	26.6	32.8	33.4	42.0	30.5	26.7	54.3	30.4	42.6	19.2	37.9	15.2	37.3	45.3	37.0
K	51.2	54.4	58.5	51.4	68.3	60.9	59.4	38.1	65.2	68.1	38.0	65.1	44.8	70.4	57.2	57.5	58.1	49.9	61.3
K/Rb	219.1	255.5	287.0	229.3	230.8	367.3	175.5	228.0	257.3	289.8	415.1	344.1	310.5	364.9	287.7	205.9	306.6	398.6	366.9
K/Ba	25.96	27.21	24.74	27.21	49.84	23.76	159.61	19.08	53.48	70.32	43.48	175.55	39.68	44.99	46.53	35.90	41.01	72.80	70.06
Ti/Zr	2.2	2.3	2.1	3.2	10.6	11.8	5.1	32.5	1.5	6.4	31.0		2.1	29.1	3.7	76.3	3.0	3.7	4.2
Ba/Sr	16.21	17.32	14.12	13.04	5.42	9.19	8.28	10.18	5.14	11.48	7.50	2.67	3.57	6.95	4.17	2.16	11.57	7.79	25.41
Rb/Sr	1.92	1.84	1.22	1.55	1.17	0.60	7.53	0.85	1.07	2.79	0.79	1.36	0.45	0.86	0.67	0.38	1.55	1.42	4.85
Ce/La	1.05	3.96	2.27	1.58	1.83	1.88	2.92	1.56	5.33	1.85	1.75	2.56	1.40	1.65	2.29	1.00	1.64	2.09	1.57
Ba/Rb	8.44	9.39	11.60	8.43	4.63	15.45	1.10	11.95	4.81	4.12	9.55	1.96	8.03	8.11	6.18	5.74	7.48	5.48	5.24

* Element not detected.
† Index = ($\frac{1}{3}$Si+K)−(Ca+Mg).

Granodiorite dyke
1. Z.602.3d, 2. Z.602.3e — Hatch Plain, Dutoit Nunataks, western Read Mountains.

Augen-gneiss
3. Z.599.2, 4. Z.599.3 — 6 km west of The Ark, western Read Mountains.
5. Z.862.1 — The Ark, western Read Mountains.
6. Z.880.1, 7. Z.880.1 — North-east corner of Beche Blade, Read Mountains. (Duplicate pair.)
8. Z.712.1, 9. Z.712.2 — Central Bernhardi Heights, Herbert Mountains.

Granite
10. Z.594.1, 11. Z.594.5, 12. Z.594.7, 13. Z.855.1, 14. Z.859.1, 15. Z.860.1, 16. Z.861.1, 17. Z.861.1 — The pluton between The Ark and Watts Needle, western Read Mountains. (16, 17: Duplicate pair.)
18. Z.602.1, 19. Z.687.1, 20. Z.688.1, 21. Z.691.1 — The pluton at Hatch Plain, Dutoit Nunataks, western Read Mountains.

Migmatite neosomes, Read Mountains
22. Z.870.1 Holmes Summit.
23. Z.880.2 North-eastern Beche Blade.
24. Z.603.3 Poldervaart Edge.
25. Z.595.3 North of Watts Needle.
26. Z.596.2 North of Watts Needle.
27. Z.692.4 6 km west of The Ark.
28. Z.863.2 Holmes Summit.
29. Z.869.2 Holmes Summit.

Migmatite neosomes, Read Mountains
30. Z.789.1 North-eastern Murchison Cirque.
31. Z.880.4 North-eastern Beche Blade.
32. Z.895.2 Escarpment north of Mount Wegener.
33. Z.600.1 North-eastern Glen Glacier.
34. Z.685.2 Hatch Plain.
35. Z.871.1 North-west of Holmes Summit.
36. Z.885.1 Between Arkel and Eskola Cirques.
37. Z.896.2 North-western Bowen Cirque.

Migmatite neosomes, Herbert Mountains and Lagrange Nunataks
38. Z.717.1 Kendall Basin.
39. Z.921.1 Charlesworth Cliffs.
40. Z.922.1 Charlesworth Cliffs.
41. Z.923.1 Charlesworth Cliffs.
42. Z.723.2 Southern Morris Hills.
43. Z.725.5 Northern Morris Hills.
44. Z.727.1 Mount Beney.
45. Z.729.3 6 km west of Mount Etchells.
46. Z.731.3 1 km north-west of Butterfly Knoll.

Migmatite neosomes, Otter and Haskard Highlands
47. Z.553.9 North of Pointer Nunatak.
48. Z.554.2 East of Pointer Nunatak.
49. Z.563.8 Lister Heights.
50. Z.566.4 Pointer Nunatak.
51. Z.826.1 North of Pointer Nunatak.
52. Z.831.6 North of Pointer Nunatak.
53. Z.844.5 Williams Ridge.
54. Z.1005.11 South of Mount Gass.
55. Z.1010.5 Mount Gass.
56. Z.1032.2 South-west of Mount Provender.
57. Z.572.1 Mount Homard.
58. Z.755.1 Mount Homard.
59. Z.795.2 South of Mount Homard.

[face page 278

Geochemistry

Fifty-nine chemical analyses of granodiorite, augen-gneiss, granite and migmatite neosomes are given in Table I. Various graphs and triangular diagrams are used to demonstrate the evolution of the intrusive sequence and the relationships between the different rock types.

The plots of the major oxides against the modified Larsen index (Nockolds and Allen, 1953) show typical values and trends for the acid end of an alkaline rock series (Fig. 17). Certain trends, notably that of CaO, are tight and regular, whereas others show more variation. Individual analyses which stand apart from the trend for a given oxide are not consistently anomalous in other oxide trends, suggesting overall conformity within the sequence. Trace elements, similarly plotted (Fig. 18), show less well-defined trends or no trend at all but some elements are present to definite levels within a rock type or a group of types from a restricted area, e.g. the Ni content of acid rocks is generally less than 13 ppm, whereas the augen-gneisses and the granodiorite dyke contain 17 ppm or more; a similar distinction can be seen with Cr. The trend in Zr is a gradual decrease with increasing acidity of the rocks except for some of the more acid migmatite neosomes with remarkably high Zr contents; Y and Ce show patterns of similar proportions but this is less obvious in Nb and La. In all these graphs, the granite plutons tend towards regularity and uniformity, with rare exceptions, but the augen-gneisses and migmatite neosomes are more variable; the two granodiorite dyke analyses cannot be reliably compared in this respect.

The triangular diagram of normative quartz and alkali-feldspar (Fig. 19a) shows that the majority of the analyses fall within the 20–60% triangle of granitic composition (Tuttle and Bowen, 1958). In the normative feldspar triangular diagram (Fig. 19b) the majority of the analyses plot within the region of the "average granite" at the albite end of the low-temperature trough (Tuttle and Bowen, 1958). One granite analysis stands alone in these

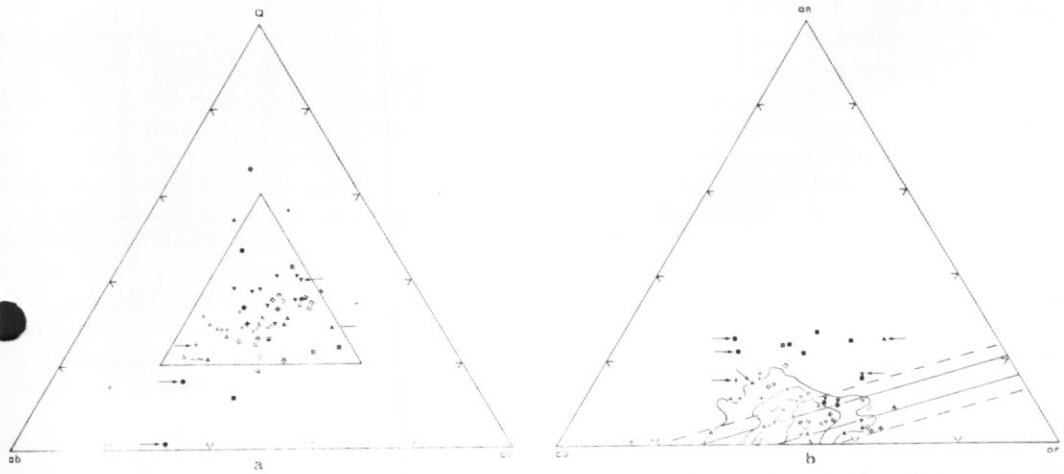

Fig. 19. a. Triangular diagram for analyses of granodiorite, augen-gneiss, granite and migmatite neosomes on the coordinates Q–or–ab (normative values). Arrows indicate analyses in which Q+or+ab<80%. The inner triangle of 20–60% indicates the field of granitic composition (after Tuttle and Bowen, 1958).
The symbols are as in Fig. 17.

b. Triangular diagram for analyses of granodiorite, augen-gneiss, granite and migmatite neosomes on the coordinates an–or–ab (normative values). The arrows indicate analyses in which Q+or+ab< 80%. The solid lines mark the boundaries of the low-temperature trough of the or–ab–an–SiO_2 system (after Tuttle and Bowen, 1958) and the dashed lines show the uncertainty due to analytical error (after Kleeman, 1965). The contours (after Tuttle and Bowen, 1958) are for 1 269 analyses of rocks with Q+or+ab≥80%. The symbols are as in Fig. 17.

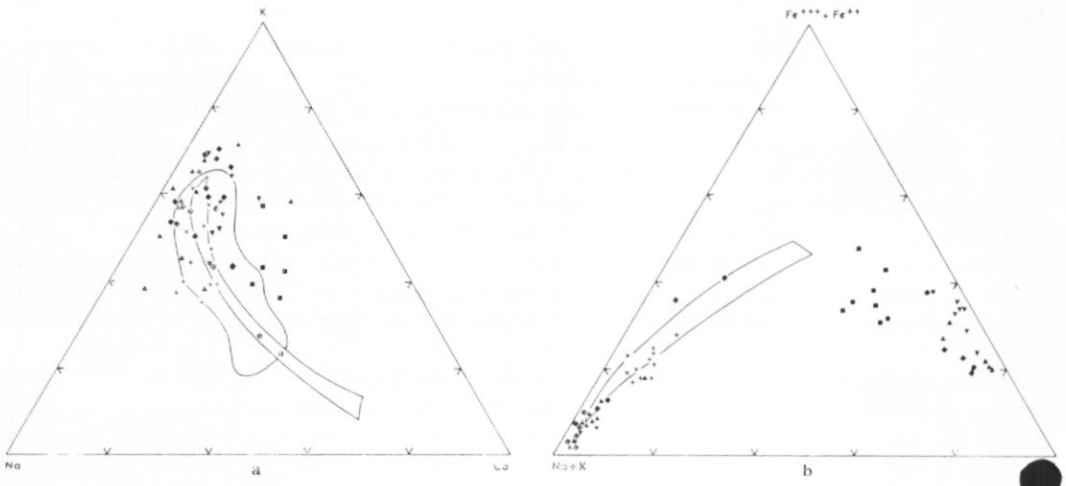

Fig. 20. a. Triangular variation diagram for analyses of granodiorite, augen-gneiss, granite and migmatite neosomes on the coordinates K–Ca–Na (weight %). The field of magmatic granites is shown (after Raju and Rao, 1972) and the major calc-alkali trend limits are outlined (after Nockolds and Allen, 1953).
The symbols are as in Fig. 17.

b. Triangular variation diagram for analyses of granodiorite, augen-gneiss, granite and migmatite neosomes on the coordinates $(Fe^{+++}+Fe^{++})$–Mg–(Na+K) (weight %). The major calc-alkali trend limits are outlined (after Nockolds and Allen, 1953).
The symbols are as in Fig. 17.

diagrams and the analyses of the augen-gneisses and the granodiorite dyke plot in the plagioclase field.

In the two variation diagrams (Fig. 20a and b) there is a degree of alignment between the plots of these analyses and the main calc-alkali trends figured by Nockolds and Allen (1953), particularly by the granites; between the other analyses there is a considerable spread and many migmatite neosomes, as well as the granodiorite dyke and the augen-gneisses, are poor in alkalis and rich in magnesium (Fig. 20b). These analyses fall in the region of accumulative rocks which Nockolds and Allen (1953) suggested may be the result of enrichment in early formed ferromagnesian minerals and/or plagioclase feldspar. However, in this case it may also be due to contamination as the neosomes in this group are markedly rich in the immobile elements Zr and Y, possibly indicating a sedimentary origin (Taylor, 1965). Most of the granite and migmatite neosome analyses fall within the field of magmatic granites (Fig. 20a), although this does not necessarily imply a magmatic origin, but those analyses outside this field should be replacement rocks, within an 80% confidence limit (Raju and Rao, 1972). The evidence of this diagram is far from conclusive but it may indicate anatexis and intrusion at a higher level.

The graphs of element ratios plotted against the modified Larsen index (Fig. 21) show the trends of changing ratios which should indicate the degree of fractionation and possibly the order of intrusion. The slopes of these graphs indicate slight fractionation but in the reverse direction to normal fractionation trends from basic to acid magma in a granitic sequence (e.g. Cobbing and Pitcher, 1972).

The K/Rb ratio normally falls with increasing fractionation and similarly indicates the order of intrusion (Taylor, 1965). In this intrusive sequence the only known field evidence for intrusive relationships is the granodiorite dyke intruding the granite at Hatch Plain. If this relationship is extrapolated, following the chemistry of the rocks, the order of intrusion is migmatite neosomes followed by granite (augen-gneiss) and then granodiorite. This is

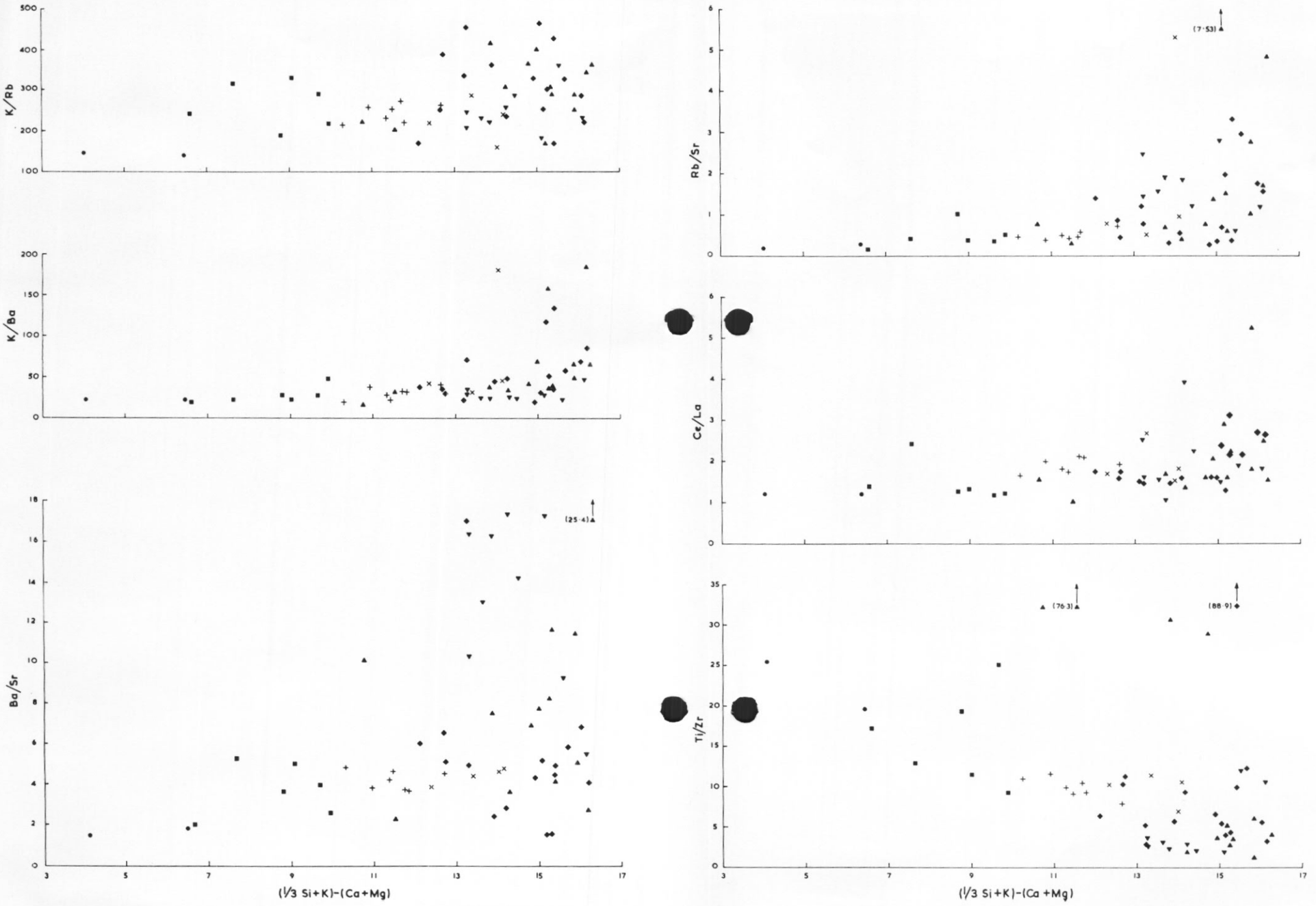

Fig. 21. Plots of various element ratios for analyses of granodiorite, augen-gneiss, granite and migmatite neosomes against the modified Larsen index (after Nockolds and Allen, 1953).
The symbols are as in Fig. 17.

[face page 278

also the trend of decreasing K/Rb ratio, which is opposite to the normal fractionation sense. Thus, either the K/Rb ratio is not a valid indicator in this rock sequence, and neither are the other ratios except Rb/Sr, or the magma has evolved from acid to basic. A third possibility could be that the granodiorite dyke, which controls the chemical trends, is not related to the granites and the migmatite neosomes which show only slight changes in ratio trends, although the ratios are frequently variable. However, the minimal marginal effects between the granite and the granodiorite dyke may indicate a close relationship with the migmatization in time as well as space. Therefore, this dyke is regarded as belonging to the same magma series and, in any case, the acid rocks do trend in the same manner, although less obviously, even without the continuation of the trend shown by the augen-gneiss and granodiorite analyses.

The K/Rb ratio normally falls with increasing fractionation and Taylor (1965) has quoted mean values for the ratio of 230 for granodiorite and 200 for granite. For this rock series, either K must decrease or Rb increase with time for K/Rb ratio to fall with time; in fact, K decreases and Rb, although very variable, shows a slight overall increase (Figs 18 and 19).

Partial melting of acid or intermediate gneisses would give rise to an acid magma with a more basic residue or restite (Mehnert, 1971). The K/Rb ratio of this magma should fall with fractionation but its acidity should increase. If the less fractionated magma is removed from the magma chamber and intruded at higher levels in the crust, the remaining more fractionated, more acid magma can only become more basic by further melting of the original gneiss. If the K/Rb ratio of the original gneiss is constant, the K/Rb ratio of the magma will still fall with increasing fractionation and further melting while becoming more basic. Similarly, as more mafic minerals are melted, the K content of the magma will decrease. However, to melt the more basic fractions of the original gneiss requires more heat and higher temperatures so that increasing temperature is a vital requirement for this process. Also, the increasing basicity of the magma will be accelerated by a continual drain of magma from the zone of melting.

The other element ratios showing recognizable trends (Fig. 21) follow the reverse of normal fractionation trends like the K/Rb ratio, but the Rb/Sr ratios behave in a normal fashion and increase with fractionation and magma acidity. Because the Rb content of the rocks is generally constant or slightly increasing with time, Sr must necessarily increase markedly for the Rb/Sr ratio to decrease. Sr will inevitably increase as Ca increases and the magma becomes more basic with increasing anorthite content of the plagioclase. This increase of Sr with Ca (Fig. 22a) and the variability of Rb and Sr in the migmatites (Fig. 22b) are both well illustrated.

Drury (1972) suggested that highly fractionated granitic material should have high Zr, Ba, La, Ce and Th contents but low Ce/La ratios. These criteria can be seen in many of the neosome analyses, particularly in the northern and western areas, but these rocks are not thought to be highly fractionated; such high immobile element contents are probably due to anatexis of original sedimentary material (Taylor, 1965). Some of these analyses also plot in the region of the accumulative rocks (Fig. 20b) of Nockolds and Allen (1953) and the diagrams of Le Maitre (1976) also showed concentrations of granitic rocks in the same region of this diagram.

The augen-gneisses with large potash feldspar porphyroblasts are considered to be the products of potash metasomatism. In this respect, they may be regarded as basic gneisses with added potash and they may be similar in composition to the residual melt after the removal of the acid components, i.e. an acid or intermediate gneiss depleted in acidic phases. They could, therefore, plot as a late stage in the anatectic sequence, although their true time of formation in the sequence is not known. The K/Rb ratios suggest early formation of the augen but, as the analyses are of whole rocks only, and not of separated feldspar augen, the inference is unreliable.

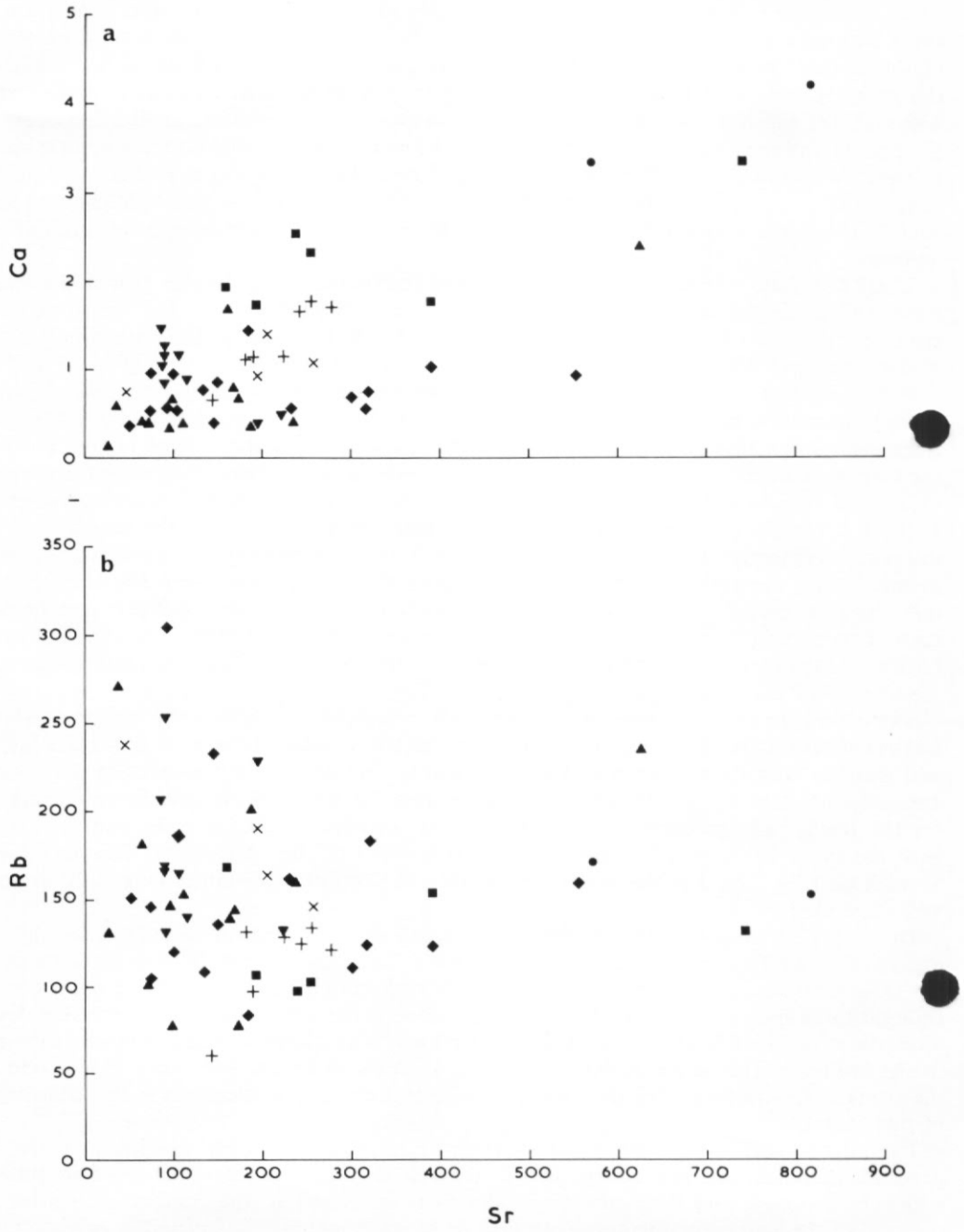

Fig. 22. Plots of Ca^{++} (weight %) and Rb (ppm) against Sr (ppm) for analyses of granodiorite, augen-gneiss, granite and migmatite neosomes.
The symbols are as in Fig. 17.

Conclusions

The probable sequence of events as interpreted above is:

i. With rising temperature, partial melting of intermediate or acid gneisses produces a granitic magma which is fractionated and injected into higher crustal levels as a migmatite neosome.
ii. With continued rising temperature, an increasing amount of mafic material is melted and the neosome acidity is slightly reduced. About this time, a series of magmatic pulses into a region of low pressure or stress produces the granite plutons.
iii. Still greater temperatures melt more basic material and the acidity of the magma decreases to a final level and the granodiorite dyke is intruded.
iv. The time of potash metasomatism and the formation of the augen in the basic gneisses is not known, although early or probably initial metasomatism is suspected; analysis of separated feldspar augen may indicate the position of the metasomatism in the anatectic sequence.

The most important mechanism involved in this sequence of intrusions is the continued [illegible] in temperature, accompanied by gradual and continual removal of magma from the "magma chamber". Increasing pressure would lead to more melting by depression of the melting points of the various minerals and would encourage emptying of the "magma chamber"; it also increases the Ab/Or ratio, thereby reducing the acidity of the magma (Brown and Fyfe, 1970). Fractionation probably took place in the initial stages of magma formation when there may have also been some crystal accumulation of early formed ferromagnesian minerals and/or plagioclase feldspar. Fractionation at other times is difficult to determine due to the reversed trends shown by this sequence. However, if a "magma chamber" existed, continued fractionation would be possible except that increasing temperature would tend to re-melt the fractionated crystalline phases and the melting of more basic material would tend to mask the fractionation effects.

A similar sequence of rock types has been predicted by the experimental work of von Platen (1965) on the anatexis of sedimentary rocks. He demonstrated that the final stage of anatexis will be granodiorite when melting a greywacke or a carbonate-rich clay. Kolbe and Taylor (1966) described granodiorites and gneissic granites, which they considered to be the products of anatexis of clay-rich and geosynclinal sediments. King (1965) has emphasized the opposite trend of such sequences when compared with the fractionation trends which produce the commoner gabbro-granite series. However, fractionation is the product of a cooling history following the initial formation of a magma, whereas the migmatization considered here is the product of a heating history providing a continual source of magma. Brown and Fyfe (1970) demonstrated magma evolution from granodiorite to granite with [illegible]creasing pressure and temperature but noted that liquids are more dioritic at higher temperatures. von Platen (1965) produced a similar range of compositions by melting gneiss and, with Winkler (Winkler and von Platen, 1961), showed that rising temperature on a greywacke produced a rock series from aplite through granite to granodiorite.

Criteria necessary for migmatite genesis by isochemical metamorphic differentiation include a similar plagioclase composition in both the palaeosome and the neosome, Q/Ab ratios not plotting around a cotectic line and the neosome to be lacking in orthoclase and a eutectic composition (Amit and Eyal, 1976). These criteria are not evident in the migmatites of the Shackleton Range.

The migmatites of the Shackleton Range Metamorphic Complex are the product of partial melting or anatexis with increasing temperature (metatexis followed by diatexis) and continual intrusion at higher levels in the crust. Potash metasomatism was probably the initial stage followed by the intrusion of the migmatite neosomes, then the granite plutons and finally the granodiorite dyke. It is not known how closely in time the migmatization was related to

the regional metamorphism of the palaeosomes but the wide development of intrusive agmatites indicates that the palaeosomes were in a plastic or mobile state. This may imply that the migmatization was a fairly deep-seated event, particularly since the granites are not sufficiently fractionated to be considered high-level granites.

The older metamorphic event and the migmatization were followed by the deposition of a sequence of arenaceous and calcareous sediments, which were subsequently metamorphosed to amphibolite facies. Some of the amphibolites may be metamorphosed basic intrusions, but this is not certain. The present distribution of rock types in the basement complex throughout the Shackleton Range is probably due to unexposed faulting and thrusting.

ACKNOWLEDGEMENTS

I wish to thank Professors F. W. Shotton and A. Williams for providing facilities in the Department of Geological Sciences, University of Birmingham, Drs G. L. Hendry, S. D. Weaver, A. D. Saunders and D. Millward for much help with the geochemical analyses, and Dr R. J. Adie for advice during preparation of this paper. I am indebted to R. B. Wyeth and M. J. Skidmore for permission to use their rock collections and field data which contributed greatly to the work. I am grateful to all my field companions and, above all, to the US N[redacted] Squadron VXE-6 without whose transport facilities this work would not have been done.

MS received 4 January 1978

REFERENCES

AMIT, O. *and* Y. EYAL. 1976. The genesis of Wadi Magrish migmatites (N-E Sinai). *Contr. Miner. Petrol.* (*Beitr. Miner. Petrogr.*), **59**, No. 1, 95–110.

BROWN, G. C. *and* W. S. FYFE. 1970. The production of granite melts during ultrametamorphism. *Contr. Miner. Petrol.* (*Beitr. Miner. Petrogr.*), **28**, No. 3, 310–18.

CLARKSON, P. D. 1972. Geology of the Shackleton Range: a preliminary report. *British Antarctic Survey Bulletin*, No. 31, 1–15.

———. 1982*a*. Geology of the Shackleton Range: II. The Turnpike Bluff Group. *British Antarctic Survey Bulletin*, No. 52.

———. 1982*b*. Geology of the Shackleton Range: IV. The dolerite dykes. *British Antarctic Survey Bulletin*, No. 53, 201–12.

———. *and* R. B. WYETH. 1981. Geology of the Shackleton Range: III. The Blaiklock Glacier Group. *British Antarctic Survey Bulletin*, No. 52.

COBBING, E. J. *and* W. S. PITCHER. 1972. The coastal batholith of central Peru. *J. geol. Soc. Lond.*, **128**, Pt. 5, 421–51.

DEER, W. A., HOWIE, R. A. *and* J. ZUSSMAN. 1966. *An introduction to the rock-forming minerals*. London, Longmans, Green and Co. Limited.

DRURY, S. A. 1972. The chemistry of some granitic veins from the Lewisian of Coll and Tiree, Argyllshire, Scotland. *Chem. Geol.*, **9**, No. 3, 175–93.

JUCKES, L. M. 1972. The geology of north-eastern Heimefrontfjella, Dronning Maud Land. *British Antarc[redacted] Survey Scientific Reports*, No. 65, 44 pp.

KAMINUMA, K. *and* M. ISHIDA. 1971. Earthquake activity in Antarctica. *Antarctic Rec.*, No. 42, 53–60.

KING, B. C. 1965. The nature and origin of migmatites: metasomatism or anatexis. (*In* PITCHER, W. S. *and* G. W. FLINN, *ed. Controls of metamorphism. A symposium held under the auspices of The Liverpool Geological Society*. Edinburgh and London, Oliver & Boyd, 219–34.) [*Geological Journal*, Special issue No. 1.]

KLEEMAN, A. W. 1965. The origin of granitic magmas. *J. geol. Soc. Aust.*, **12**, Pt. 1, 35–52.

KOLBE, P. *and* S. R. TAYLOR. 1966. Major and trace element relationships in granodiorites and granites from Australia and South Africa. *Contr. Miner. Petrol.* (*Beitr. Miner. Petrogr.*), **12**, No. 2, 202–22.

LE MAITRE, R. W. 1976. The chemical variability of some common igneous rocks. *J. Petrology*, **17**, Pt. 4, 589–637.

MACKENZIE, W. S. 1957. The crystalline modifications of $NaAlSi_3O_8$. *Am. J. Sci.*, **255**, No. 7, 481–516.

MEHNERT, K. R. 1971. *Developments in petrology. Vol. 1. Migmatites and the origin of granitic rocks*. 2nd impression. Amsterdam, London, New York, Elsevier Publishing Company.

NOCKOLDS, S. R. *and* R. ALLEN. 1953. The geochemistry of some igneous rock series. *Geochim. cosmochim. Acta*, **4**, No. 3, 105–42.

RAJU, R. D. *and* J. S. R. K. RAO. 1972. Chemical distinction between replacement and magmatic rocks. *Contr. Miner. Petrol.* (*Beitr. Miner. Petrogr.*), **35**, No. 2, 169–72.

REX, D. C. 1971. K-Ar age determinations on volcanic and associated rocks from the Antarctic Peninsula and Dronning Maud Land. (*In* ADIE, R. J., *ed. Antarctic geology and geophysics*. Oslo, Universitetsforlaget, 133–36.)

ROOTS, E. F. 1953. Preliminary note on the geology of western Dronning Maud Land. *Norsk geol. Tidsskr.*, **32,** Ht. 1, 18–33.

———. 1969. Geology of western Queen Maud Land (Sheet 6, western Queen Maud Land). (*In* BUSHNELL, V. C. *and* C. CRADDOCK, *ed.* Geologic maps of Antarctica. *Antarct. Map Folio Ser.*, Folio 12, Pl. VI.)

SPRY, A. 1969. *Metamorphic textures*. Oxford, London, Edinburgh, etc., Pergamon Press.

STEPHENSON, P. J. 1966. Geology. 1. Theron Mountains, Shackleton Range and Whichaway Nunataks (with a section on palaeomagnetism of the dolerite intrusions, by D. J. Blundell). *Scient. Rep. transantarct. Exped.*, No. 8, 79 pp.

TAYLOR, S. R. 1965. The application of trace element data to problems in petrology. (*In* AHRENS, L. H., PRESS, F., RUNCORN, S. K. *and* H. C. UREY, *ed. Physics and chemistry of the Earth*, **6.** Oxford, London, Edinburgh, New York, Paris, Frankfurt, Pergamon Press, 133–213.)

THOMSON, J. W. 1968. Petrography of some Basement Complex rocks from Tottanfjella, Dronning Maud Land. *British Antarctic Survey Bulletin*, No. 17, 59–72.

TURNER, F. J. *and* J. VERHOOGEN. 1960. *Igneous and metamorphic petrology*. 2nd edition. New York, Toronto and London, McGraw-Hill Book Company, Inc.

TUTTLE, O. F. *and* N. L. BOWEN. 1958. Origin of granite in the light of experimental studies in the system $NaAlSi_3O_8$–$KAlSi_3O_8$–SiO_2–H_2O. *Mem. geol. Soc. Am.*, No. 74, 153 pp.

VON PLATEN, H. 1965. Experimental anatexis and genesis of migmatites. (*In* PITCHER, W. S. *and* G. W. FLINN, *ed. Controls of metamorphism. A symposium held under the auspices of The Liverpool Geological Society*. Edinburgh and London, Oliver & Boyd, 203–18.) [*Geological Journal*, Special issue No. 1.]

WINKLER, H. G. F. *and* H. VON PLATEN. 1961. Experimentelle Gesteinsmetamorphose—V. Experimentelle anatektische Schmelzen und ihre petrogenetische Bedeutung. *Geochim. cosmochim. Acta*, **24,** Nos. 3/4, 250–59.

WORSFOLD, R. J. 1967. *The geology of southern Heimefrontfjella, Dronning Maud Land*. Ph.D. thesis, University of Birmingham, 176 pp. [Unpublished.]